Environmental Modelling and Software 197 (2026) 106845

Contents lists available at ScienceDirect

Environmental Modelling and Software

journal homepage: www.elsevier.com/locate/envsoft

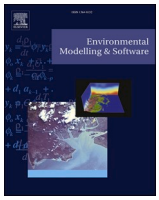

A coupled land use change-ecohydrological model for multi-seasonal arid agricultural systems: an Egyptian case study

Aimen Sattar [a,*], Simon Moulds [b], Calum Brown [c,e], Mark Rounsevell [b,c,d], Peter Alexander [a,b]

[a] Global Academy of Agriculture and Food Security, The Royal (Dick) School of Veterinary Studies, University of Edinburgh, Easter Bush Campus, Midlothian, EH25 9RG, UK
[b] School of Geosciences, University of Edinburgh, Drummond Street, EH25 9RG, Edinburgh, UK
[c] Institute of Meteorology and Climate Research, Atmospheric Environmental Research (IMK-IFU), Karlsruhe Institute of Technology, Kreuzeckbahnstraße 19, 82467, Garmisch-Partenkirchen, Germany
[d] Institute for Geography and Geo-ecology, Karlsruhe Institute of Technology, Kaiserstraße 12, 76131, Karlsruhe, Germany
[e] Highlands Rewilding Ltd., The Old Schoolhouse, Inverness, IV63 6XG, UK

ARTICLE INFO

Keywords:
Coupled modelling
Crop yield
Water use
CO_2 fertilisation
Adaptation
Arid agriculture

ABSTRACT

Modelling interactions between climate, water, crops, and human decision-making requires coupling of biophysical and socioeconomic processes to model outcomes and explore potential futures. This study presents a novel coupled model of land-use change and ecohydrological processes in arid agricultural systems. The model links SWAT+, which simulates ecohydrological processes, including crop growth and irrigation water use, with CRAFTY, an agent-based framework that allocates land according to agent characteristics and resource conditions. Egypt is used as a case study where climate and socioeconomic stressors constrain agricultural production. The coupling captures how shifts in potential yields, driven by elevated CO_2 and warming, shape land-use change. Crop yields vary by crop and scenario, with the largest gains – and declines – under high-emission futures, while water use efficiency consistently improves, especially at higher CO_2 concentrations. Relying on open global datasets, the model provides a transferable approach for exploring climate adaptation in data-scarce, water-limited regions.

1. Introduction

Climate change poses significant risks to environmental and socio-economic systems, particularly for land use and freshwater management (Z. Cao et al., 2022). The agricultural sector, as the largest global user of both land and freshwater, is especially vulnerable (Malhi et al., 2021). These vulnerabilities include more frequent and extreme weather events, shrinking arable land area, declining soil quality, and rising crop water demand; trends which are already occurring rapidly in arid and semi-arid agricultural systems (El-Beltagy and Madkour, 2012). Climate change has already reduced global agricultural productivity by an estimated 21 % since 1961 compared to a no-climate-change baseline, with higher losses in some of the most climate-exposed regions, including Sub-Saharan Africa (34 %), and the Middle East and North Africa (30 %) (Ortiz-Bobea et al., 2021). However, the net impact remains uncertain due to the potential counteracting effect of elevated CO_2, which may enhance photosynthesis and water use efficiency for some crops under certain conditions (Ainsworth and Long, 2021; Jägermeyr et al., 2021). As the rate and severity of climate change are likely to increase over the coming decades (Zittis et al., 2022), proactive adaptation remains essential to manage risks, sustain agricultural productivity and capitalise on the benefits to some crops (Grigorieva et al., 2023).

The responses of governments and farmers to constrained freshwater resources and the impacts of climate change on water and land systems are crucial for both farmer welfare and food and water security (Grigorieva et al., 2023). Agricultural activity in arid and semi-arid regions has long been defined by its ability to meet these challenges (El-Beltagy and Madkour, 2012). Whether or not it continues to do so is likely to be determined by the interaction of hydrological and land-use systems, and the extent to which they can be influenced by agricultural management decisions at various spatial scales. It is therefore essential to understand the dynamics of these complex systems, predict how they may change in the future, and assess the efficacy of policies for natural resource management, food and water security, and rural development

* Corresponding author.
E-mail address: A.M.A.Sattar@sms.ed.ac.uk (A. Sattar).

https://doi.org/10.1016/j.envsoft.2025.106845
Received 16 August 2025; Received in revised form 17 November 2025; Accepted 22 December 2025
Available online 26 December 2025

(Alam et al., 2022).

A wide range of modelling approaches have been used to assess agricultural responses to climate and socioeconomic change, each with distinct strengths and limitations. Econometric models capture statistical relationships between climate variables and yields, often assuming profit-maximising behaviour, but they lack spatial and behavioural detail (Feng et al., 2023; Su and Chen, 2022). More sophisticated economic models, such as computable general equilibrium (CGE) models, can capture economy-wide impacts of agricultural change but struggle to represent physical constraints and heterogeneity in farmer behaviour (Huber et al., 2018). Physical models, including crop and hydrological models, simulate biophysical processes such as photosynthesis, transpiration, and runoff generation with high resolution and are useful for analysing yield and water impacts under climate change (Dlamini et al., 2023; You et al., 2024). However, they typically represent cropping decisions and water management as static or uniform, limiting their ability to account for local adaptation (Alam et al., 2022; McDermid et al., 2023). Addressing these limitations, agent-based models (ABMs) simulate heterogeneous decision-making in response to changing environmental and socioeconomic conditions, and are particularly useful in arid regions where farm-level decisions shape water use outcomes (Alam et al., 2022; Schrieks et al., 2021). However, their effectiveness depends on their ability to be adequately calibrated and on the availability of spatially and behaviourally rich data, which can be challenging in data-scarce contexts (Brown et al., 2023; Kimpton et al., 2024).

Recent advances in agricultural systems modelling reflect a growing recognition of the need to capture feedback between climate, water, crop growth, and human decision-making. Increasingly, models are coupling biophysical processes and socioeconomic behaviour to improve the realism and relevance of climate impact assessments (e.g. Canales et al., 2024; Mijic et al., 2023; Streefkerk et al., 2023). These integrated models are particularly relevant to arid and semi-arid contexts, where agricultural outcomes are tightly constrained by both environmental stressors and adaptive management strategies (El Fartassi et al., 2025; Harms et al., 2023). Coupled models allow for the simultaneous analysis of yields, water demand and behavioural responses, dimensions which are often addressed separately in standalone crop, hydrological, or agent-based models (El Fartassi et al., 2025; O'Keeffe et al., 2018). Recent work has improved the representation of irrigation and crop-water interactions in arid environments (e.g., Elsayed et al. (2025)), yet these models generally operate at field or watershed scales and do not integrate dynamic land-use or behavioural responses. Existing coupled approaches, therefore, remain limited in their ability to explore long-term adaptation pathways and feedbacks across biophysical and socioeconomic systems.

Additionally, most existing coupled models focus primarily on short-term farm management decisions, particularly irrigation scheduling and technology adoption (Du et al., 2020; Harms et al., 2023; O'Keeffe et al., 2018). This limits their capacity to explore long-term adaptation pathways in arid and semi-arid systems, where shifting cropping patterns represent a crucial response to sustained climate and resource pressures. Ecohydrological models such as the Soil and Water Assessment Tool (SWAT), Agricultural Production Systems Simulator (APSIM), and AquaCrop provide detailed simulations of crop growth, hydrology, and irrigation demand, but often assume static land use and uniform management practices (Bieger et al., 2017; Holzworth et al., 2014; Steduto et al., 2009). Conversely, agent-based models, such as Competition for Resources between Agent Functional Types (CRAFTY) or mathematical programming-based multi-agent systems (MP-MAS), capture heterogeneity in decision making and resource endowments (Berger et al., 2007; Murray-Rust et al., 2014), but typically rely on externally prescribed productivity and water availability inputs, limiting their capacity to reflect feedback from environmental processes (Alam et al., 2022).

Taken together, these limitations highlight a clear research gap: the absence of long-term, transferable coupled models that can jointly simulate land-use change, irrigation behaviour, and biophysical feedbacks under changing climate and socioeconomic conditions. This gap is particularly relevant in data-scarce, multi-seasonal agricultural systems such as Egypt, where both physical processes and adaptive management strongly influence water and land outcomes. To address these limitations, we develop a novel coupled model linking biophysical and agent-based components to simulate land-use and irrigation dynamics in large, intensively managed agricultural systems. The innovation of the coupled model lies in three main aspects: (1) the explicit multi-seasonal representation of crop and irrigation processes; (2) the integration of biophysical and socioeconomic responses, allowing land-use change and irrigation behaviour to evolve interactively; and (3) the use of openly available global datasets that enable application in data-scarce regions and across a broad range of cropping patterns.

The coupled model combines SWAT+, a spatially explicit ecohydrological model (EHM) that simulates crop growth and water use, with CRAFTY, an agent-based model representing land-use decisions through agent functional types. SWAT + supports applications in data-scarce regions and has proven effective in capturing yield and water use in managed systems such as Egypt's Nile Valley and Delta (Bieger et al., 2017; Chawanda et al., 2024). CRAFTY complements this by modelling farmers' adaptive land-use responses to changes in resource access, climate, and policy drivers (Murray-Rust et al., 2014). The coupled model captures both irrigation decisions and transitions in cropping patterns and land use. By linking these two models, the coupled model enables assessment of long-term adaptation trajectories and feedbacks between land use, water demand, and climate, providing a robust and scalable approach for agricultural systems in arid and semi-arid regions.

This research presents the development and application of the coupled model. We describe the model components, coupling strategy, and input datasets. Egypt serves as a case study due to its reliance on irrigation and a multi-seasonal cropping system. The model is applied to estimate potential yield and water use trajectories under various climate change scenarios to 2099, providing insight into how future conditions may affect agricultural productivity and water demand in arid systems. We go on to apply the coupled model using static socioeconomic conditions to demonstrate the benefit of the coupling over a standalone ecohydrological model.

2. Model description

We present a novel model that implements a coupling process between biophysical and agent-based components (Fig. 1). The biophysical model (SWAT+) calculates potential crop yields under optimal management for different climate change scenarios, generating annual natural capital inputs that represent grid-cell productivity ceilings. These outputs inform the agent-based model (CRAFTY), where agricultural producers, competing through capital-weighted utility functions, determine land use patterns and management practices. Socioeconomic capitals (infrastructure access, financial resources, access to mechanisation, human resources, social cohesion, access to water resources) drive agent competition. This coupled model prioritises provisioning services such as crop production while incorporating policy objectives such as water use efficiency. Finally, the annual gridded agents derived from the competition in CRAFTY are passed onto the SWAT + model, where the land use and management practices are used to determine gridded production and water use. The coupling propagates spatial heterogeneity in water use efficiency through agent-specific irrigation strategies, with commercial agents adopting modern techniques and subsistence agents persisting with traditional practices.

2.1. SWAT + biophysical model

We use the SWAT + model, a semi-distributed watershed ecohydrological model (Arnold et al., 1998), to simulate biophysical processes. The SWAT + model simulates hydrology and crop production at a regional scale. SWAT + builds on the original SWAT model, offering

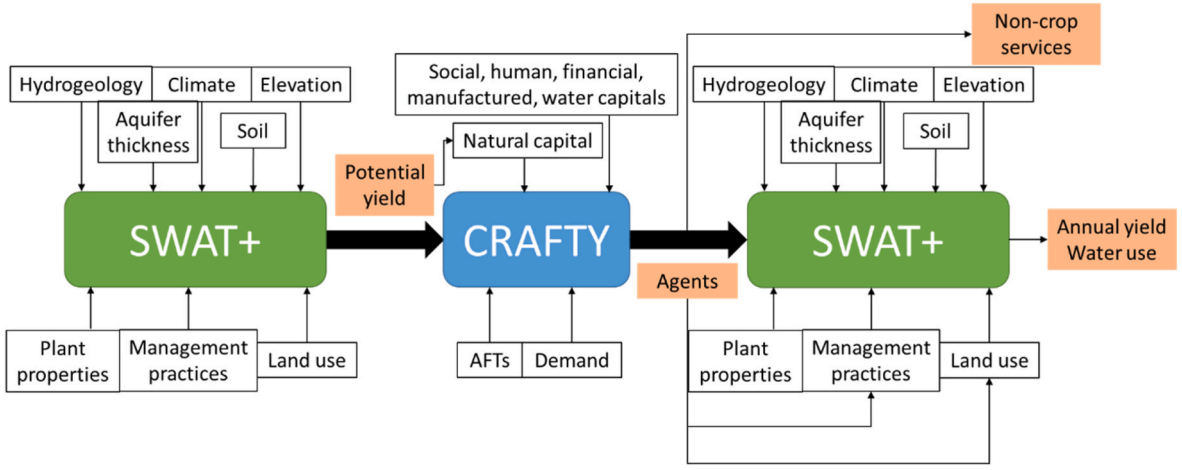

Fig. 1. Conceptual framework of the coupled land-use change-ecohydrological (LUC-EH) model. SWAT+ is shown twice to represent its two sequential roles: first simulating potential yields for CRAFTY inputs, and then simulating realised yields and water use based on CRAFTY outputs. The figure illustrates the general data flow between models.

enhanced flexibility in model component configuration and spatial discretisation (Bieger et al., 2017). It simulates hydrology and crop growth processes across large regions by linking subbasins, defined by topography, with hydrological response units (HRUs). HRUs represent homogeneous areas defined based on land use, soil type, and slope. Although these semi-distributed HRUs are computationally efficient, they do not include connectivity and interactions between HRUs. SWATgrid was developed to enable gridded, location-specific HRUs, which also represent watersheds, allowing for the linking of grids and routing flow between them (Pignotti et al., 2017).

Crop growth in SWAT+ is simulated using the Erosion Productivity Impact Calculator (EPIC) crop growth model (Williams et al., 1984), which provides a process-based representation of photosynthesis, transpiration, and biomass accumulation. Management practices are implemented using decision tables that define actions such as planting, harvesting, irrigation, reservoir management, fertiliser application, ploughing, and pesticide application (Arnold et al., 2018). These management activities can be scheduled by date or triggered by thresholds, such as soil water content, plant water stress, or accumulated plant heat units. The decision table structure allows simulation of diverse crop and irrigation practices, including the automation of irrigation based on crop water requirements and the availability of water from surface or groundwater sources. The flexibility of the decision table structure also supports seasonal and perennial systems, as well as fixed calendars and rules tied to environmental triggers. Combined with its comprehensive library of plant types and default agronomic parameters, SWAT + remains accessible for applications in data-scarce regions. Full details of the decision tables as they are applied in SWAT + are included in Arnold et al. (2018).

To estimate potential yields, we implement the biophysical model under optimal management assumptions. Irrigation is triggered automatically when soil moisture falls below field capacity, applying sufficient water as per crop water demand, ensuring non-stressed crop growth. Fertiliser is also applied based on nutrient stress to ensure non-limiting growth conditions. This approach prioritises yield maximisation, which is the required input for the CRAFTY natural capital layer, and represents common practices in low-income irrigated systems, simplifying operation variations such as Egypt's dominant flood irrigation (Abdelhafez et al., 2020). Additionally, tree crops (fruit/date) are assumed to be at full maturity. Other multi-year perennial crops, such as sugarcane, are simplified and harvested and replanted on an annual basis to facilitate annual land-use change.

Elevated atmospheric CO_2 concentrations under future climate scenarios are also an important aspect of crop modelling. Elevated CO_2 levels can enhance crop growth through the carbon fertilisation effect, which increases photosynthetic and water use efficiencies (Wang et al., 2017). SWAT + incorporates this effect through adjustments in the EPIC crop model, where crop transpiration and biomass accumulation respond dynamically to prescribed CO_2 concentrations, typically aligned to Representative Concentration Pathways (RCPs) (Meinshausen et al., 2020; Zhang et al., 2022). The model uses a radiation use efficiency (RUE) approach to simulate crop growth, with RUE specified at both ambient and elevated CO_2 levels. Default parameters are available for many crops within SWAT+'s plant database (plants.plt), facilitating implementation in data-scarce regions where crop-specific trial data may not be available. These built-in features support consistent incorporation of CO_2 fertilisation effects across diverse crop and climate scenarios (USDA Agricultural Research Service, 2020).

2.2. CRAFTY agent-based model

The agent-based component of the coupled model is implemented using the Competition for Resources between Agent Functional Types (CRAFTY) framework (Murray-Rust et al., 2014). The CRAFTY framework has been applied to various contexts, including Sweden (Blanco et al., 2017), Europe (Brown et al., 2019), Great Britain (Brown et al., 2022), and Brazil (Millington et al., 2021). CRAFTY models the production of ecosystem services by agents utilising spatially explicit resources (capitals) (Murray-Rust et al., 2014). Competition between Agent Functional Types (AFTs) reflects how land use and management practices evolve. Their competitiveness is determined by a utility function that incorporates unmet demand and a Cobb–Douglas production function. AFTs are defined based on the distribution of "give in" and "give up" thresholds and their capital sensitivities. The "give in" threshold represents the agent's willingness to yield to competition, while the "give up" threshold represents the agent's likelihood to relinquish land if they are not profitable (Murray-Rust et al., 2014). The capital sensitivities describe how sensitive an AFT is to a resource in the production of an ecosystem service.

2.3. Model coupling of SWAT+ and CRAFTY

In the coupled model, information flows sequentially between SWAT+ and CRAFTY. Initially, SWAT+ is employed to simulate crop growth and water use for each crop type across all agricultural grid cells within the six regional models under optimal management conditions. This process determines potential yields without irrigation or fertiliser resource constraints. The potential yield for each cell and crop is

normalised by rescaling all values between the overall minimum and maximum yields across all cells, years, and scenarios, such that the minimum corresponds to 0 and the maximum to 1. The maximum yield for each cell and crop is then established as the potential yield, which is subsequently normalised for each crop type. These normalised values serve as the natural capital inputs for the CRAFTY model. Following this, the CRAFTY model simulates inter-agent competition, generating annual gridded AFTs. These AFTs can be translated into land use and management practices within SWAT+, which in turn simulate crop growth and provide annual crop production and water use results under different socioeconomic and climate change scenarios. Non-crop ecosystem services, such as employment and water use efficiency, are defined in CRAFTY.

3. Egypt case study

3.1. SWAT + model implementation for Egypt

To demonstrate the application of this coupled model, we implement SWAT + for Egypt, a highly irrigated agricultural system characterised by multi-seasonal cropping and high dependence on Nile River flows for irrigation. The model uses a daily timestep and 900 m grid resolution to model yield and water use for winter and summer crops. Model input data is summarised in Table 4. The model is structured into six separate submodels representing the Nile Delta, Nile Valley, and Mediterranean regions, collectively covering 28 % of Egypt's land area and 92 % of its cultivated land (Fig. 2 and Table A.4). Due to SWAT+'s data handling limitations for gridded models, each model is constrained to fewer than 90,000 grid cells. This segmentation ensures efficient processing while maintaining comprehensive coverage of the entire region.

We utilise statistical reports of annual land use (CAPMAS, 2025) to generate land use maps using the European Space Agency (ESA) land cover dataset (Copernicus Climate Change Service, 2019) as the underlying land cover distribution. Appendix A.1 includes details of the process used to develop the land use map in 2020. We use the total area grown for each crop in each governorate as the basis for this. As Egyptian cropping systems are highly flexible, evolving quickly, and lack fixed rotation rules, the model simplifies crop rotations to a statistically optimised set of representative winter–summer combinations. Although sequences such as Egyptian clover (berseem) followed by maize are common, they are not applied consistently across regions or years, as other crops are often substituted depending on local conditions, labour availability, market demand, and management preferences. To ensure computational feasibility and efficient model development, a minimum number of representative cropping patterns were identified using statistical optimisation based on the 2010 statistical reports of cropped areas for seasonal and perennial crops (CAPMAS, 2025). This approach captures the dominant rotational structure while keeping the model tractable. The SWAT + model inputs include crop-specific decision tables for planting, harvesting, and irrigation (summarised in Tables 1 and 2). Cropping calendars are based on regional planting and harvesting dates and heat unit thresholds.

SWAT + internally simulates both potential and actual evapotranspiration (ET) as part of the crop–water balance, based on temperature, precipitation, radiation, humidity, and wind speed. Under increasing temperatures, potential ET generally rises, while elevated CO_2 reduces stomatal conductance, which can moderate or reduce actual ET. These processes are therefore accounted for within the model structure, although ET outputs were not evaluated separately due to the limited availability of observational ET records in Egypt. For modelling potential yields, irrigation is triggered automatically when soil moisture falls below field capacity, ensuring optimal water supply to maximise crop

Table 1
Planting and harvesting decision table details for winter, summer, perennial, and tree crops.

Season	Decision	Planting	Harvesting
Winter	Date	6th November	30th April
	Heat Units	–	1.15
Summer	Date	15th May	27th October
	Heat Units	–	1.15
Perennial	Date	6th November	27th October
	Heat units	–	0.9
Trees	Date	–	15th September

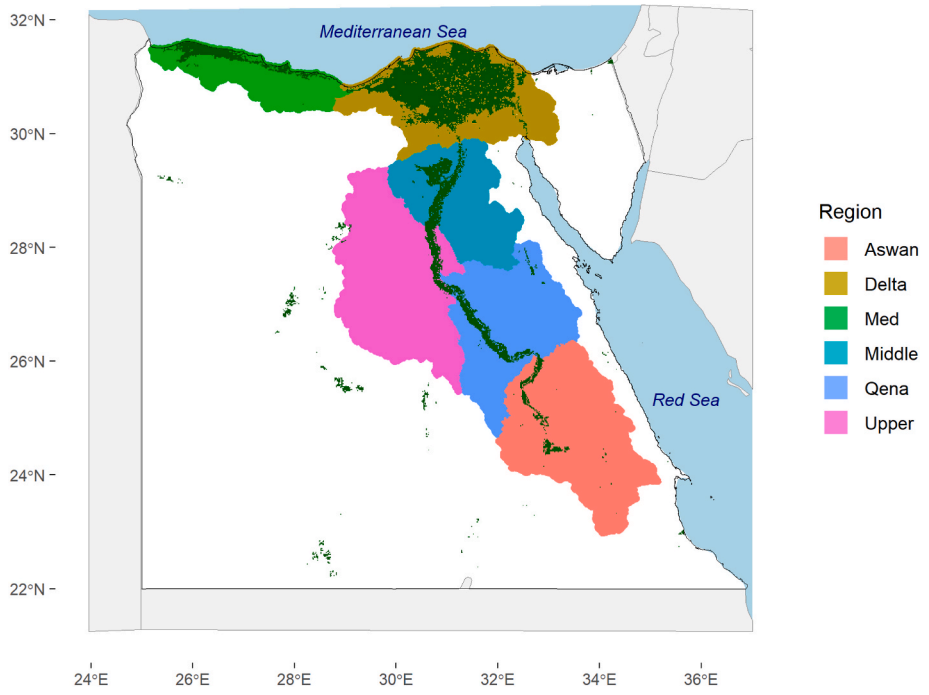

Fig. 2. Model regions and cropped area in Egypt: SWAT + submodel areas and national cropped area in 2020. The cropped area is in dark green. (For interpretation of the references to colour in this figure legend, the reader is referred to the Web version of this article.)

Table 2
Irrigation decision table details for commercial and Subsistence farmers.

Modelling stage/ Management	Method	Threshold method	Threshold quantity	Water per application
Potential yield modelling	Furrow	Soil moisture	100 %	Based on demand
Deficit irrigation	Defined per crop and region	Soil moisture/ plant water stress	Defined per crop and region	Defined per crop and region

productivity. In preparation for actual yield and water use modelling, additional irrigation settings are developed to reflect deficit irrigation strategies. These are applied during the final stage of the workflow, when land use from CRAFTY is used to drive SWAT+. In this case, irrigation is triggered by either soil moisture thresholds or plant water stress, and the volume of water applied is based on either crop water demand or specified quantities. These settings are derived through a sensitivity analysis, detailed in Section 4.1.

Multi-cut crops such as alfalfa and berseem clover are typically harvested multiple times annually under real-world conditions. Berseem and alfalfa achieve 3–7 cuts per year in Egypt (FAO, 2014), while sugarcane's perennial growth allows annual harvesting up to 5 times (Mehareb et al., 2021). Berseem and alfalfa crops are harvested based on reaching 90 % of the plant-heat units to maturity, up to four times per season, followed by a final harvest and termination. To facilitate annual land-use change modelling, sugarcane is simplified to a single-year growth and harvest cycle. Perennial crops are assumed to align with winter cropping calendars, with termination occurring 10 days before replanting. Fruit and date trees, modelled at full maturity, follow fixed annual harvests on 15th September to reflect simplified regional practices.

While a detailed analysis of fertiliser impacts is beyond this study's scope, calibration requires fertilisation to be defined. The Food and Agriculture Organization of the United Nations (FAO) report on crop-specific fertiliser use in Egypt (Food and Agriculture Organization of the United Nations, 2005) provides estimates of fertiliser use for each crop in Egypt. This is used in the initial phase of the modelling to allow for calibration of the model. Fertiliser application is defined using the same decision table structure, with automatic application triggered by nutrient stress. The default crop-specific fertiliser setting is included in Table A.3.

To maintain hydrological continuity across the modelled domain, a cascading configuration is implemented for the Nile Valley and Delta submodels. In this setup, the outlet of each upstream region serves as the inlet for the downstream model, thereby replicating the natural flow progression of the Nile River and enabling a coherent simulation of water movement across regions. While the model does not calibrate streamflow explicitly – owing to the simplified representation of Egypt's irrigation system, in which irrigation water is applied from an abstract, unlimited source – streamflow values are based on historical records (Hou et al., 2024). Streamflow projections are estimated by averaging values across the historical period and extending them uniformly to 2100. The Mediterranean submodel is excluded from the cascading configuration due to the absence of major upstream inflows.

3.2. CRAFTY model implementation for Egypt

We apply the CRAFTY framework to Egypt to model the process of land-use change through competition between AFTs. CRAFTY-Egypt uses a 900 m × 900 m resolution grid and is developed to simulate land use change between 2020 and 2100. The model is comprised of capitals, which represent the spatially explicit resources. These include socioeconomic capitals – manufactured, human, social and financial. Table 5 contains details of the indicators used for each of these capitals.

Table 3
Yield and irrigation application parameters, method of change, minimum and maximum value range and whether the variable is model-wide or crop-specific. Change: abschng = absolute change of value, percent = percentage change, replace = replace value. Parameters: bm_e.plt = biomass-energy ratio, tmp_pot.plt = optimal temperature for plant growth, tmp_base.plt = minimum temperature for plant growth, harv_idx.plt = harvest index for optimal growth conditions, lai_pot.plt = maxium potential leaf area index, phu_mat.plt = plant heat units to maturity, esco.hru = soil evaporation compensation factor, cn2.hru = Condition II curve number, perco.hru = percolation coefficient, awc.sol = available water capacity of the soil layer, surlag.bsn = surface runoff lag coefficient, aquifer_delay.hru = delay time for groundwater flow to stream.

Observed data	Parameter	Change	Min	Max	Details
Yield	bm_e.plt	abschng	−5	5	Crop specific
Yield	tmp_opt.plt	abschng	−3	3	Crop specific
Yield	tmp_base.plt	abschng	−1	1	Crop specific
Yield	harv_idx.plt	percent	−70	70	Crop specific
Yield	lai_pot.plt	percent	−70	70	Crop specific
Yield	phu_mat.plt	percent	−70	70	Crop specific
Irrigation	esco.hru	replace	0	1	Model
Irrigation	cn2.hru	percent	−70	70	Model
Irrigation	perco.hru	replace	0.01	1	Model
Irrigation	awc.sol	percent	−70	70	Model
Irrigation	surlag.bsn	replace	0.05	24	Model
Irrigation	aquifer_delay.hru	replace	0	1000	Model

Each distributed indicator is sampled to the base grid of the model, so for every model grid cell, there is a value for each year. The indicators are scaled between 0 and 1 and summed for each grid to develop the capitals. The indicators use a range of spatial resolutions. The education and health indices (Smits and Permanyer, 2019), farm machinery prevalence, and per capita membership of agricultural cooperatives (CAPMAS, 2025) are governorate-level datasets. GDP per capita is calculated using 1 km^2 resolution gridded GDP and population datasets (Wang and Sun, 2022; Wang et al., 2022). The population and GDP gridded values are scaled to account for updated projections (Koch and Leimbach, 2023). These datasets are then resampled at 900 m × 900 m resolution to match the model resolution. We define human capital by summing the health and education indices and scaling the values by gridded population data. Gridded GDP per capita is used to represent the financial capital. Social capital is represented by the combination of per capita membership in agricultural cooperatives (CAPMAS, 2025) and the Gini index (OAMDI, 2023), as higher income inequality – measured by the Gini index – is associated with lower levels of social cohesion and trust within communities (Delhey et al., 2023; Tucker and Xu, 2023). Finally, manufactured capital is derived from gridded road infrastructure data (Meijer et al., 2018) and governorate-level agricultural machinery per unit agricultural area (CAPMAS, 2025).

The representation of water availability in the model necessitated the explicit inclusion of a *water capital* variable. While Egypt is classified as a highly water-stressed nation due to its limited renewable freshwater resources (Gado and El-Agha, 2021), this scarcity primarily reflects current technological and infrastructural constraints rather than absolute physical limits. Non-renewable water sources – including fossil groundwater reserves, wastewater reuse, and desalination – hold the potential to expand freshwater access significantly under future technological advancements. As the model is designed for scenario analysis, water capital is conceptualised not as a fixed physical quantity but as a dynamic measure of *access to water,* contingent on technological capacity and infrastructure development. This capital is integrated in the model using three spatially explicit components: (1) rainfall patterns

Table 4
Input data used to develop the SWAT + model.

Submodel	Data	Spatial resolution	Temporal resolution	References
Global datasets				
Surface water	MERIT DEM	90m	–	Yamazaki et al. (2017)
	ESA Landcover	300m	Annual (2020)	Copernicus Climate Change Service (2019)
	DSOLMap	250m	–	(Hengl et al., 2017; López-Ballesteros et al., 2023)
	Lake shapefile		–	Messager et al. (2016)
	Streamflow			Hou et al. (2024)
	CO_2 concentration		2020–2100	Meinshausen et al. (2020)
Groundwater	Soil grid depth to bedrock	250m	–	Hengl et al. (2017)
	GLHYMPS			(Gleeson, 2018; Huscroft et al., 2018)
Climate data	Climate data bias corrected and downscaled for MRI-ESM2-0 climate model: rainfall, min/max temperature, relative humidity, solar radiation, wind speed	0.25° (25 km at the equator)	Daily	(Lange and Büchner, 2021; Yukimoto et al., 2019)
National datasets				
Cropping pattern	2010 cropped areas	governorate	Annual (2010–2019)	CAPMAS (2025)
Calibration	Yield data	Governorate		CAPMAS (2025)
	Water use data	Governorate		CAPMAS (2025)

derived from climate projections (Lange and Büchner, 2021), (2) proximity to surface water infrastructure, mapped via open-source geospatial datasets (Humanitarian OpenStreetMap Team (HOT), 2024; Messager et al., 2016), and (3) the hydraulic head of confined groundwater aquifers, which governs extraction feasibility (Verkaik et al., 2024). By integrating these factors, the model captures both natural hydrological constraints and human-mediated water accessibility, enabling robust exploration of future scenarios where technological innovations reduce costs or enhance efficiency in non-renewable water exploitation.

In addition to capitals, the CRAFTY framework includes AFTs, which represent land managers. Our application of the framework has 56 AFTs, which characterise different cropping patterns and management practices. Although not direct representations of the farming household types described in Sattar et al. (2024), our model draws loosely on their typology to define two broad agent categories: Commercial (inspired by specialised households) and Subsistence (based on village households), in line with the model's objectives. All cropping patterns are represented by both agent types to reflect variation in management strategies.

The cropping patterns in Egypt are not fixed. Some crops are only grown in a specific season – Winter: legumes, wheat; Summer: maize, fibre, rice, oil crops – whilst others can be grown in both seasons. The final cropping patterns are estimated based on annual production and area reports (CAPMAS, 2025). As the seasonal data is not available for 2020, the 2010 seasonal areas are used. Crops are grouped based on the groupings used by the Government of Egypt in its annual production and area reports, with the most important crops for each group being used as the representative plant. Table A.1 includes details of the plant used to represent each crop grouping. Fig. 3 illustrates the relative size of different cropping patterns. It includes, on the left, the relative size (by area) of the subsistence and commercial farmers in 2020. As the diagram shows, we estimate that 10 % of the cropped areas are commercial and 90 % are subsistence. The middle section of the diagram shows the relative areas of winter crops, and finally, the right section of the diagram shows the relative areas of summer crops.

The model differentiates agricultural agents based on management practices, encoded through distinct behavioural parameters. Subsistence agents represent smallholder farmers who rely on flood irrigation and are characterised by lower income levels, limited access to technology, and strong dependence on social capital such as community networks. These agents exhibit a greater propensity to persist with agricultural production even under economically non-competitive conditions, prioritising subsistence needs over market-driven optimisation. In contrast, commercial agents adopt market-oriented farming practices, including the use of deficit irrigation, alongside external labour, advanced technologies. The commercial AFT represents behaviour that is more responsive to poor performance, defined by a lower giving-up threshold than that of subsistence AFTs. This means that less profitable grid cells are more readily relinquished, reflecting greater responsiveness to changing conditions rather than higher overall resilience. These behavioural distinctions are systematically embedded within the model's sensitivity matrices and AFT parameters, which govern the competition (land-use change) processes. The details of how the sensitivity matrices and AFT parameters are developed for a business-as-usual scenario are included in Tables A.10 and A11.

The AFTs compete to produce ecosystem services. The Egyptian implementation of the CRAFTY framework quantifies ecosystem services across four dimensions critical to agricultural systems: crop production, water use efficiency, livestock products, and employment generation. Service provision varies according to AFT, reflecting differences in crop selection and management strategies. Crop production is universal across all agricultural agents, with each cultivating either one or two crops depending on their AFT. Water use efficiency varies between AFTs, with commercial agents achieving greater efficiency through deficit irrigation methods, whereas subsistence agents rely on traditional flood irrigation practices. Additionally, AFTs cultivating water-intensive crops (i.e. rice and fibre) exhibit reduced efficiency compared to those focusing on less water-intensive crop types.

Livestock products, including meat and milk, are generated indirectly through two pathways: by agents specialising in fodder crops (i.e. alfalfa and seasonal fodder), and via crop residues from cereal cultivation. Employment generation occurs universally but varies in magnitude, with commercial agents creating more opportunities due to the labour-intensive nature of advanced practices and larger operational scales, whilst subsistence farmers are likely to depend more on household labour.

In Egypt, agricultural expansion through land reclamation, the process of converting desert or other non-cultivated land into farmland, has been a common practice to increase agricultural production (Adriansen, 2009). Government-sponsored projects, such as those in the New Valley, prioritise desert land conversion through centralised irrigation infrastructure. Simultaneously, smallholder farmers along the Nile Valley and Delta fringes engage in informal reclamation, leveraging shallow groundwater from Nile-dependent aquifers (Nour, 2020). As the New Valley Governorate is outside the boundaries of our model, large state-sponsored projects are not included. However, to reflect the process of informal reclamation within the model, an Unmanaged Land (UL) agent is introduced. This agent is assigned to all grid cells that are neither cultivated nor masked as urban or wetland areas. Additionally,

Table 5
Input data used to develop the capital layers for the CRAFTY model.

Capital	Indicator	Details	References
Global datasets			
Human	Education index	Subnational Human Development Index indicator	Smits and Permanyer (2019)
	Health index	Subnational Human Development Index indicator	Smits and Permanyer (2019)
	Population downscaling	1 km^2 gridded population datasets resampled to 0.81 km^2 resolution. These are rescaled based on updated national population values and used to downscale human capital.	(Koch and Leimbach, 2023; Wang et al., 2022)
Manufactured	Road infrastructure inventory	Developed based on 2015 data.	Meijer et al. (2018)
Financial	GDP per capita	1 km^2 gridded GDP and population datasets resampled to 0.81 km^2 resolution. These are rescaled based on updated national GDP and population values.	(Koch and Leimbach, 2023; Wang and Sun, 2022; Wang et al., 2022)
Water Capital	Rainfall	0.25° resolution gridded daily rainfall data summed per year from data bias corrected and downscaled for MRI-ESM2-0 climate model.	(Lange and Büchner, 2021; Yukimoto et al., 2019)
	Distance to surface water infrastructure	Distance to lakes and canals calculated using surface water layer from Opens Street Map for canals and rivers.	(Humanitarian OpenStreetMap Team (HOT), 2024) Messager et al. (2016)
	Groundwater head of confined aquifer layer		Verkaik et al. (2024)
National datasets			
Social	Coop membership per capita	Governorate-level dataset	CAPMAS (2025)
	Gini index	Calculated from the Household Expenditure, Income, and Consumption Survey expenditure statistics.	Calculated from (OAMDI, 2023)
Manufactured	Tractors per feddan	Governorate-level statistics of tractors per feddan	CAPMAS (2025)
Modelled datasets			
Natural capital	Potential yield	Calculated from the SWAT + model at 900m resolution.	

due to agents' sensitivity to socioeconomic capitals, grid cells with zero socioeconomic capitals are also excluded. The UL agent represents state ownership of uncultivated land and remains in place unless displaced by a competing agricultural agent. The UL agent does not produce any ecosystem services, does not 'give-up' land, and has a 0 'give-in' threshold, thus relinquishing land to any other agent regardless of their competitiveness.

3.2.1. Demand

CRAFTY does not simulate international trade and, as such, does not represent actual demand. Instead, demand for domestic production of food, fibre, and animal products is used as a proxy for demand (included in Table A.9). In this application of the coupled model, we applied static demand values to demonstrate model functionality. These 2020 baseline values for food and fibre ecosystem services are derived from national statistical and dietary reports (CAPMAS, 2025). We used a different approach for non-food and non-fibre ecosystem services, namely employment and water-use efficiency. We estimated employment demand by multiplying the total population by the proportion employed in agriculture. Water-use efficiency is treated as an index, with a baseline value of 100 in 2020.

3.3. Coupled model implementation

After completing the CRAFTY sensitivity analysis (Section 4), we ran the CRAFTY model using static demand, business-as-usual AFT parameters and production sensitivities, and fixed socioeconomic capitals and demand based on 2020 conditions. Natural capital, however, was dynamically derived from the biophysical model simulations under RCP2.6, RCP4.5, RCP6.0, RCP7.0, and RCP8.5 climate scenarios. To account for the influence of initial conditions, the CRAFTY model was run ten times using different randomised initial land-use maps, as explained above. The model simulated land-use change and shifts in management practices, specifically irrigation, under each scenario through competition between AFTs. Outputs from these simulations were then used to drive SWAT+, which provides a more detailed and process-based representation of crop growth and water use under varying land use configurations. This stylised implementation, which holds socioeconomic capitals, demand, and AFT parameters constant, was designed to demonstrate the functionality of the coupled framework and to isolate the effects of climate and land-use change on agricultural production and water use. Future applications will incorporate dynamic socioeconomic and behavioural processes to explore adaptation and policy responses in greater detail. The coupled model is summarised in Fig. 4, and results presented in Section 6.5, below.

4. Sensitivity analysis and calibration

4.1. Sensitivity analysis and calibration of SWAT+

Calibration and validation are critical steps in ecohydrological modelling, ensuring model outputs align with observed data while understanding model uncertainty (Zou et al., 2023). For this study, the SWAT + calibration focused on two primary outputs: crop yield and irrigation water use. The process addressed data limitations through a hierarchical calibration methodology using Latin Hypercube Sampling (LHS) and targeted parameter adjustments.

The six regional submodels (encompassing the Nile Delta, Nile Valley, and Mediterranean regions) were calibrated separately to ensure model parameters are developed specifically for each region (Čerkasova et al., 2023). Due to the size of the models, it was not possible to use them directly for calibration. Smaller models were developed using a subbasin within each submodel for the calibration process. All land uses were distributed randomly and evenly across the representative regional model in cropped areas only.

Fertiliser parameters were excluded from calibration, as Egypt's agricultural practices maintain near-optimal application rates (Food and Agriculture Organization of the United Nations, 2005). Instead, fertiliser settings were adjusted during sensitivity analysis to determine maximum potential yield. Additionally, irrigation parameters were not included in the calibration. Irrigation was applied at rates sufficient to meet full crop water demand whenever soil water content fell below field capacity, representing conditions for yield maximisation under the dominant flood irrigation methods used in Egypt (Abdelhafez et al.,

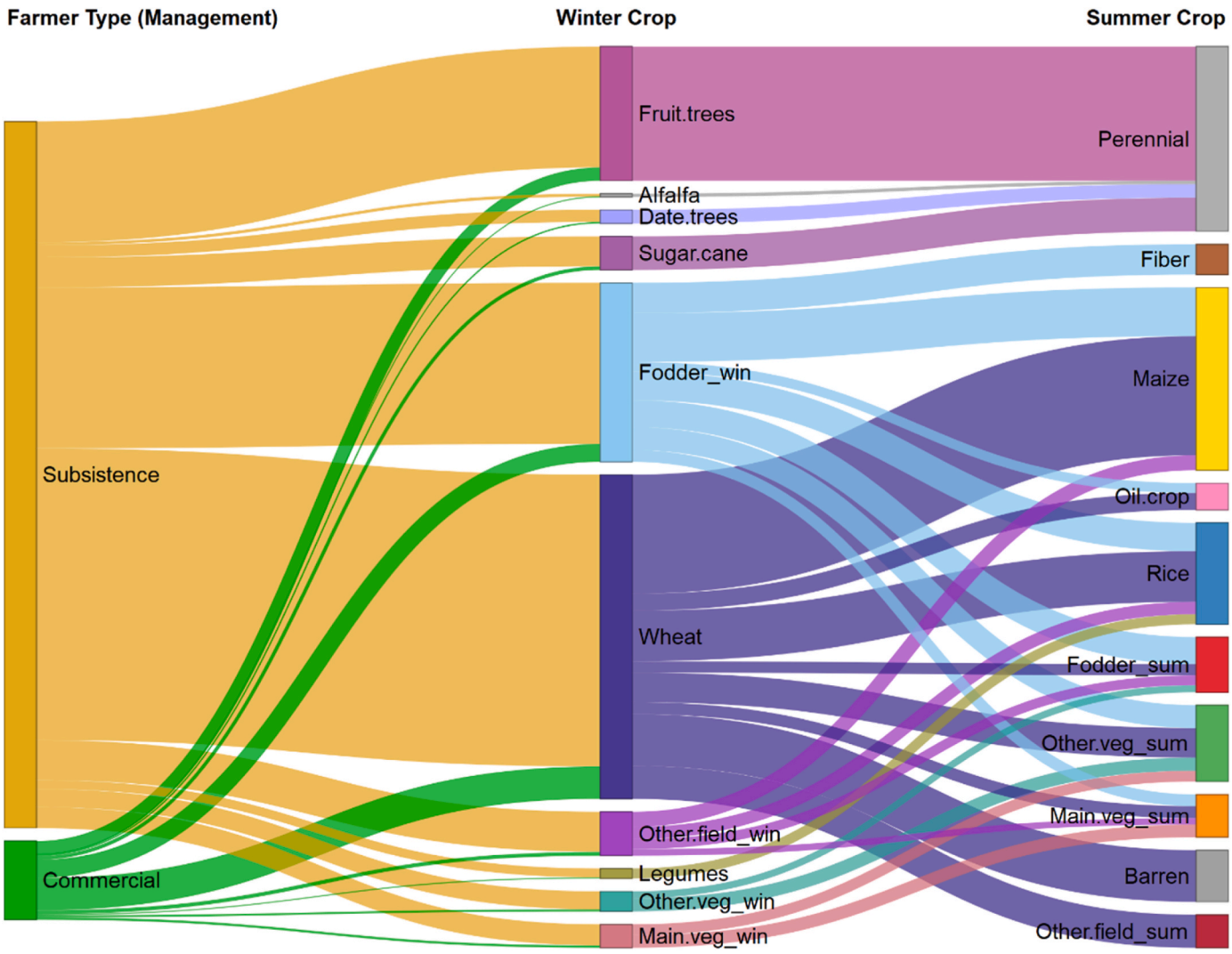

Fig. 3. Management practice, and winter and summer cropping patterns in 2020: The width represents the percentage area of each. The very left shows the division between commercial and subsistence farmers, the middle shows the crops grown in winter, and the right shows the crops grown in summer. For crops grown in both winter and summer, "_win" denotes the area in winter and "_sum" the area in summer.

2020).

The calibration prioritised parameters directly influencing crop yield and water use, as detailed in Table 3. Yield calibration focused on the optimal and base temperatures (tmp_opt and tmp_base), biomass energy conversion rate (bm_e), harvest index (harv_idx), potential leaf area index (lai_pot), and plant heat units to maturity (phu_mat). Irrigation calibration targeted parameters governing soil water dynamics, including the soil conservation service curve number (cn2), soil evaporation compensation factor (esco), percolation coefficient (perco), available soil capacity of the soil layer (awc), surface runoff lag coefficient (surlag), and aquifer delay.

We calibrate simulated average annual yield and irrigation water use against observed data, similar to the "soft calibration" method applied by Čerkasova et al. (2023), using a modified version of the RSWAT package (Nguyen et al., 2022). Observed yield and irrigation data were obtained from annual governorate-level statistical data (CAPMAS, 2025), providing regionally aggregated statistics for crops used. As crop models simulate dry matter yield, while observed yield data typically includes moisture content, we applied a range of crop-specific moisture percentages (detailed in Table A.5). During calibration, we identified whether the minimum, average, or maximum moisture content yielded the lowest error for each crop. To enable unconstrained land use transitions, all crops were included in every region's calibration. For crops not currently grown in a region, we used the average observed yield across all governorates as a proxy. ted to ensure consistency at national-scale, and so smooths field-level heterogeneity that may be more relevant for local applications.

Unlike Čerkasova et al. (2023), however, who apply plant uptake compensation factor (EPCO) – a measure of the compensation of water uptake from lower soil layers – adjustments on a HRU level, our approach requires a uniform EPCO value for each model, as the crop in each HRU will be modified in further modelling. This ensures EPCO values are suitable for all crops used in the model. Table 3 summarises the calibrated parameters, their adjustment methods (absolute change, replace or percentage change), allowable ranges, and scope (model-wide or crop-specific). A step-by-step summary of the calibration and sensitivity analysis is outlined below.

Step 1: Yield parameter calibration

We use a Latin Hypercube Sampling (LHS) ensemble of 10,000 parameter sets per region to calibrate crop-specific growth parameters. After filtering parameter sets for those within 25 % of the lowest normalised root mean square error (NRMSE) value, we evaluated model performance using a weighted scoring metric prioritising error reduction (50 % NRMSE, 25 % PBIAS) while retaining explanatory power (25

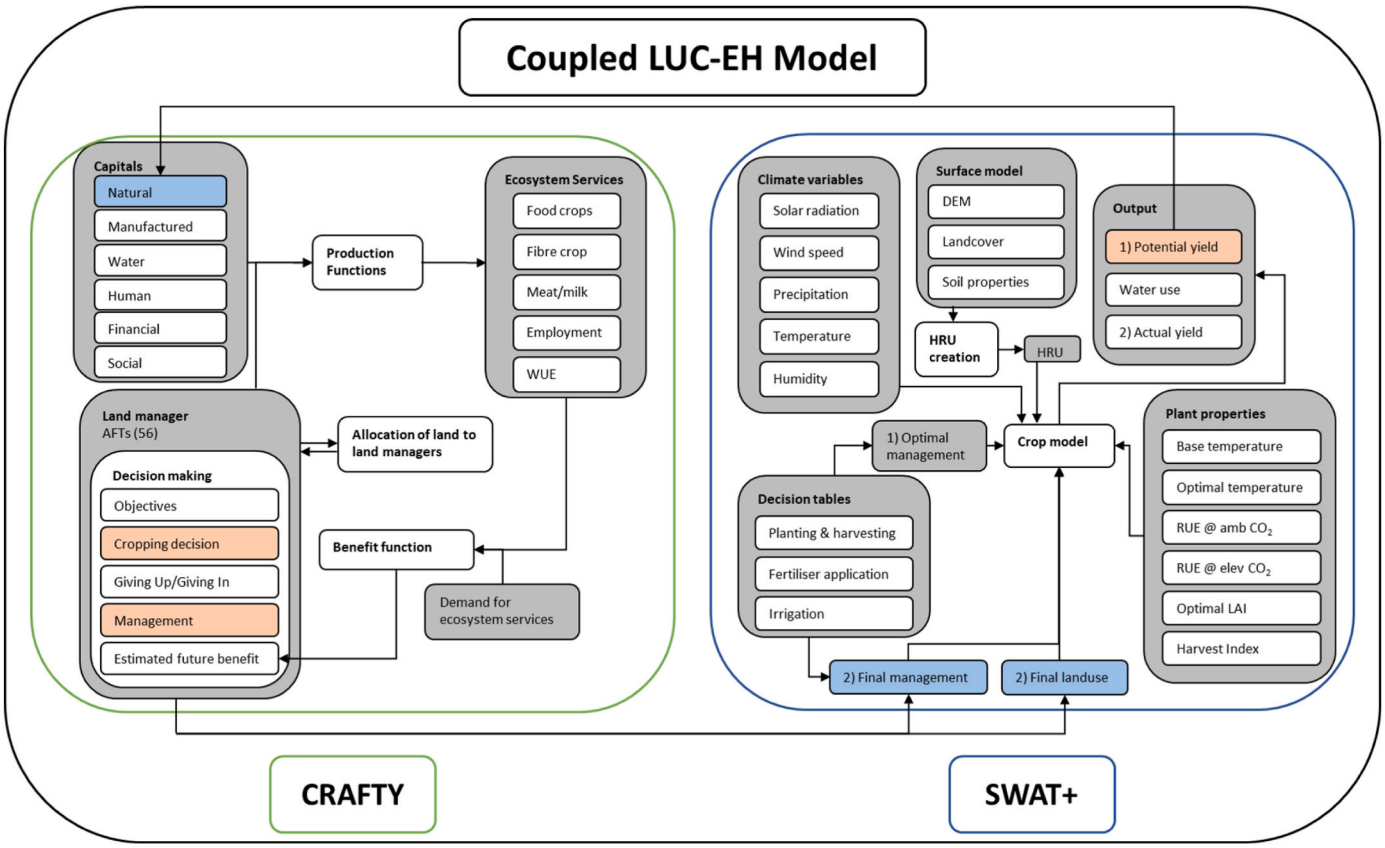

Fig. 4. Coupled LUC-EH model schematic for Egypt: The diagram shows information exchange between CRAFTY (left) and SWAT+ (right) as implemented in the Egypt case study. Orange boxes represent model outputs passed as inputs (blue) to the other model. In SWAT+, Step 1 refers to the initial run simulating potential yield, and Step 2 uses land use and management from CRAFTY to simulate actual yield and water use. The schematic has been simplified to include the most relevant aspects of each model (especially SWAT+) to the coupled model and does not include, for example, many hydrological features of the SWAT + model. (For interpretation of the references to colour in this figure legend, the reader is referred to the Web version of this article.)

% R^2). To reduce the changes to the default values, we also add a penalty for the parameters, with lower deviation from default values being preferred. The optimal parameter combination for each crop in each region was selected based on this composite score.

Step 2: Irrigation water use calibration

A subsequent LHS ensemble of 10,000 parameter sets was used to optimise irrigation variables, with water use per unit area in Egypt's simplified irrigation zones (Upper, Middle, and Lower regions) serving as the observed dataset. In the initial filtering step, we retained only those runs whose yield NRMSE was within 25 % of the best-performing run, ensuring that irrigation calibration did not come at the cost of yield accuracy. The remaining runs were then ranked using a multi-criterion scoring system weighted 75 % towards NRMSE and 25 % towards R^2, allowing us to balance calibration accuracy against the model's stylised representation of irrigation.

Step 3: Fertiliser sensitivity for maximum yield

Fertiliser application rates and stress thresholds were systematically adjusted to identify configurations maximising simulated yields. This aligned with Egypt's high-input farming norms, where nitrogen application typically ranges 200–300 kg/ha (Food and Agriculture Organization of the United Nations, 2005). The resulting parameters defined potential yields under idealised nutrient conditions.

Step 4: Deficit irrigation analysis

A similar sensitivity analysis identified irrigation strategies that reduced water use relative to yield penalties $\leq$10 %. We iteratively adjusted parameters governing irrigation triggers (soil water deficit and plant water stress thresholds) and application volumes and frequencies to map trade-offs between water conservation and productivity.

4.2. Sensitivity analysis of CRAFTY

Within CRAFTY, the natural capital layers, as defined by potential yields, have the greatest influence on ecosystem service supply. To a lesser extent, ecosystem services are also influenced by the socioeconomic capitals. At model initialisation, the CRAFTY model automatically scales demand to match the modelled supply, therefore preserving the supply provided from the biophysical model, removing the need for further calibration. Model evaluation is primarily carried out via analysis of the sensitivity of the model output to parameter values, in line with previous applications of the model (e.g. Blanco et al., 2017; Brown et al., 2022), while evaluation of the model framework itself ensures appropriate functioning (Brown et al., 2023).

The sensitivity analysis entails modifying the AFT parameters ('giving-in' and 'giving-up') and production sensitivity tables for socioeconomic capitals to determine their impact on the supply of ecosystem services. This is completed for a single scenario representing the business-as-usual case. The socioeconomic capitals are held constant at 2020 levels during the analysis, while natural capitals reflect potential yields under the same scenario. To further assess the influence of sensitivities, an additional run was conducted where all socioeconomic capital sensitivity values or all AFT parameters were set to zero. Due to the model size and time required for each run, a one-at-a-time sensitivity analysis is adopted (Pianosi et al., 2016).

The initial distribution of land use was based on a random allocation of crops, informed by land cover satellite data and governorate-level statistics on cropped areas for each crop. While this ensures accuracy at the administrative level, it does not necessarily reflect field-level patterns. To account for the potential influence of initial conditions, the model was run ten times with different initial land-use distributions, and results were aggregated across these runs for reporting.

5. Data

Developing ecohydrological models requires a large, diverse dataset to characterise the physical characteristics of the model area. The absence of good-quality, open-source, national GIS datasets necessitated the use of global datasets. National data was used for cropped areas and yields. Table 4 includes details of the data used to drive and parameterise the SWAT + model of Egypt. Table 5 includes details of the data used to create the CRAFTY model of Egypt. Global datasets, which can be utilised for different regional applications of the coupled model, are separated from national and modelled data that are specific to the model application for Egypt.

6. Results

6.1. SWAT + calibration analysis

Calibration performance varied by crop and region. In the Delta region (Fig. 5), wheat and oil crops both achieved strong agreement with observed yields, each with an R^2 of 0.67 and NRMSE values of 24 % and

Table 6
Average yield calibration and validation NRMSE, R^2, and PBIAS for each region.

Region	Calibration			Validation		
	R^2	NRMSE (%)	PBIAS (%)	R^2	NRMSE (%)	PBIAS (%)
Aswan	0.51	44.14	2.77	0.12	91.24	18.80
Delta	0.46	32.79	0.38	0.18	98.08	10.56
Med	0.59	34.52	2.46	0.34	97.22	13.64
Middle	0.44	44.90	1.83	0.14	101.37	8.48
Qena	0.47	72.01	2.23	0.31	114.86	10.43
Upper	0.66	35.55	1.10	0.43	145.56	14.02
Average	**0.52**	**43.98**	**1.79**	**0.25**	**108.19**	**12.65**

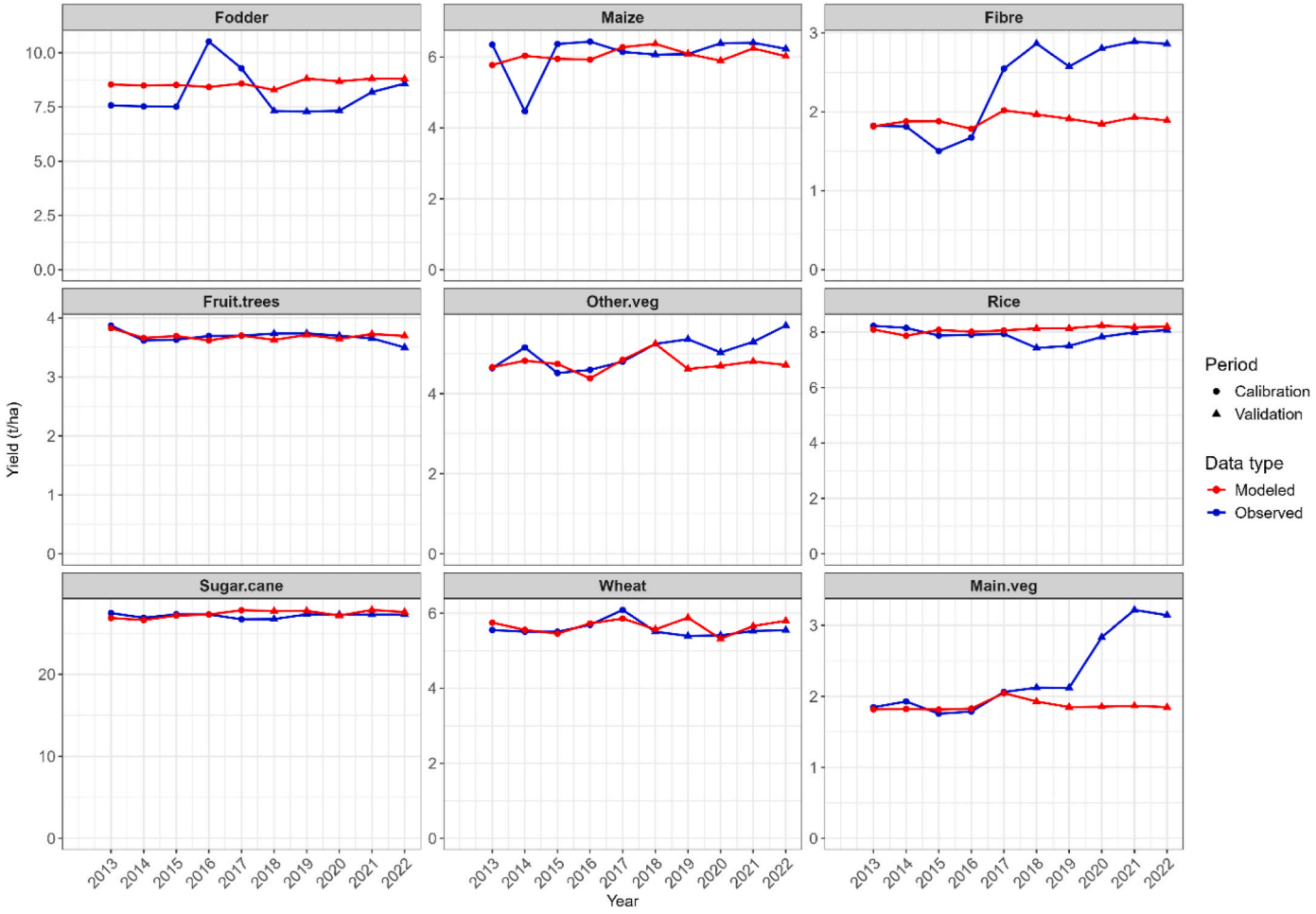

Fig. 5. Yield calibration and validation plots for key crops for the Delta region: Observed dry yield in blue and modelled dry yield in red. The calibration period (2013–2017) and the validation period (2018–2022) are represented by a circle and a triangle, respectively. (For interpretation of the references to colour in this figure legend, the reader is referred to the Web version of this article.)

29 %, respectively. Maize also produced relatively accurate yield magnitudes, with an NRMSE of 33 %, but its low R^2 of 0.30 indicates limited ability to capture interannual variability. Performance declined slightly during validation. On average, R^2 dropped from 0.52 in calibration to 0.25 in validation, while NRMSE increased from 44 % to 108 % (Table 6). However, although absolute PBIAS increases from 1.79 % to 12.65 % in calibration and validation stages, it remains below 15 % showing that systematic bias is acceptable during the validation stage.

Performance also varied by region. The Mediterranean region recorded the lowest calibration error ($R^2 = 0.59$, NRMSE = 34.52 %), while the Upper region achieved the strongest model fit ($R^2 = 0.66$, NRMSE = 35.55 %). Qena exhibited the weakest performance, particularly during calibration ($R^2 = 0.47$, NRMSE = 72.01 %). These patterns persisted into the validation phase, where regions that calibrated well tended to validate more reliably. Full calibration and validation plots for all crops and regions are provided in the Supplementary Materials.

6.2. Sensitivity analyses

6.2.1. Fertiliser sensitivity analysis

The fertiliser sensitivity analysis revealed that for many crops and regions, the default nutrient application settings were already optimal for yield. This was particularly evident for crops such as alfalfa, seasonal fodder, legumes, oil crops, and fibre, where no improvements in average yield were observed through further fertiliser adjustments. However, for other crops – particularly sugarcane, rice, other vegetables, and wheat – adjusting fertiliser inputs improved performance, with sugarcane consistently showing the highest yields under high nitrogen and phosphorus input scenarios. Notably, maize and rice responded strongly to reduced nitrogen stress, but excessive phosphorus application often showed diminishing returns.

6.2.2. Irrigation sensitivity analysis

The irrigation sensitivity analysis aimed to identify deficit irrigation configurations that achieved water savings while maintaining yield losses within an acceptable 10 % threshold. On average across all regions and crops, water use was reduced by approximately 51 %, while yield declined by only 6.7 %, confirming the effectiveness of the selected settings. Some systems showed particularly efficient trade-offs: for instance, legumes and winter other vegetables (winter potatoes) achieved water savings of 76 % and 72 %, respectively, with yield reductions of 4.01 % and 5.49 %, respectively. Conversely, sugarcane and date trees experienced lower irrigation reductions (25 % and 26 %), with yield reductions of 5.00 % and 7.47 %, respectively. The highest yield reduction was exhibited by winter seasonal fodder (9.15 %), which resulted in an irrigation reduction of 54 %.

6.2.3. CRAFTY sensitivity analysis

The analysis of the CRAFTY model's sensitivity to changes in socio-economic capital sensitivities showed a moderate response (detailed results included in Appendix B). Higher capital sensitivities led to lower production of most crop-related ecosystem services, while animal products, employment, and water use efficiency were less affected. This pattern was consistent with the sensitivity analysis of AFT parameters.

Fig. 6. Projected yield trajectories for key crops under different climate scenarios (2020–2099): Yield values are based on modelled outputs for currently cultivated lands only, illustrating changes over time for each crop and scenario.

Regarding abandonment and agricultural expansion, differences between sensitivity runs were relatively limited. The minimum abandoned area was 41,472 ha, compared to a maximum of 58,806 ha. Abandonment was higher when AFT parameters were at their lowest. However, when the 'give-up' probability or the sensitivity to capitals was set to zero, abandonment was lowest. Reclamation of unmanaged land, which varied across runs from 247,698 ha to 382,644 ha, followed a similar pattern: the smallest reclaimed area occurred when AFT parameters were at their lowest, while the highest reclamation occurred when the 'give-up' probability or sensitivity to capitals was set to zero.

6.3. Potential yields under different climate scenarios

Model outputs show varying yield responses across crops and climate scenarios (Fig. 6). Fodder crops, including seasonal fodder and alfalfa, demonstrate the largest percentage increases between 2020 and 2099, with gains of 119 % and 117 %, respectively. Wheat also shows a marked increase under RCP8.5, with average yields in currently cultivated areas rising by over 43 %. This represents a 36 % increase in 5-year average yield (2095–2099 vs. 2020–2024), reaching approximately 9 t/ha by the end of the century.

Main vegetables and sugarcane also exhibit strong yield gains of 25 % and 34 % between 2020 and 2099, respectively. In contrast, maize, fibre crops, and rice display non-linear trends under RCP8.5, with yields peaking between 2060 and 2080 before declining towards 2099. Fruit tree yields remain relatively stable, with modest increases between 4 % and 13 % across scenarios based on the 5-year average comparison. The greatest reduction in yield was observed for other vegetables, which reduces by 31 % between 2020 and 2099, under the RCP8.5 scenario. Overall, RCP8.5 leads to the greatest gains, with a 25 % increase in yield across all crops. By comparison, under RCP2.6, yields remain relatively stable, with an average increase of just 4 % over the century.

Yield responses also vary spatially. Under all climate scenarios, maize yields decline across much of Egypt by the late 21st century, with reductions of up to 25 % in some areas, particularly in the southern region (Fig. 7b). In contrast, wheat yields increase in all scenarios and across all regions (Fig. 7a), with the most pronounced gains in currently uncultivated areas of the Western Desert (Upper Egypt SWAT + submodel), where increases of up to 75 % are projected.

A noticeable spatial distinction emerges between currently irrigated areas in the Nile Valley and Delta and newly cultivated zones. For both wheat and maize, currently irrigated areas maintain higher yields across all scenarios, except in the case of wheat under RCP8.5, where new expansion areas also experience marked gains.

6.4. Water use efficiency

Water use efficiency (WUE) in old lands (Fig. 8) shows considerable variation across climate scenarios under assumptions of ideal irrigation and optimal fertiliser application. The most substantial improvements are observed under RCP8.5, which leads to an average 69 % reduction in water use per tonne of yield across all crops. Alfalfa and seasonal fodder exhibit the greatest improvements, reducing water use by 88 % and 85 %, respectively. Sugarcane and wheat also benefit, with water use reductions of 79 % and 75 % between 2020 and 2099.

In contrast, RCP2.6 shows minimal gains, with an average WUE improvement of just 4 % over the same period. For other vegetables, WUE remains relatively stable across most scenarios, with a slight increase in water use per tonne of 0.6 % under RCP2.6 and a modest decrease of 2.1 % under RCP7.0. However, RCP8.5 again stands out, reducing water use for this crop group by 47 %.

Most crops follow a consistent trend of improvement, with the magnitude of gains increasing along the scenario severity gradient: RCP2.6 (−4 %), RCP4.5 (−16 %), RCP6.0 (−21 %), RCP7.0 (−32 %), and RCP8.5 showing the greatest improvement in WUE.

6.5. Land use change

The implementation of the coupled model reveals notable variations in crop areas and production levels across scenarios (Fig. 9). Seasonal fodder, wheat, sugarcane, and main vegetables all show increased production under RCP4.5, RCP7.0, RCP6.0, and RCP8.5. Among these, seasonal fodder experiences the most substantial rise, increasing from 130 Mt in 2020 to 255 Mt in 2100 under RCP8.5. In contrast, RCP2.6 results in either stable or slightly declining production levels for these crops. Despite rising production, cropped areas for seasonal fodder, wheat, and main vegetables show gradual declines across all scenarios.

Fibre crops, rice, and maize exhibit non-linear trends under RCP8.5, peaking around 2070 before declining towards the end of the century. Other vegetables initially decline to 7.44 Mt before increasing again to reach 10.0 Mt by 2100. The area under other vegetables also expands markedly between 2080 and 2099, from 568,851 ha to 817,493 ha.

Patterns in abandoned land (Appendix A.4) are consistent across all scenarios except RCP8.5, which shows a sharp decline in abandonment after 2080, reaching 21,708 ha by 2099. In other scenarios, abandonment increases gradually, ranging from 43,092 ha (RCP7.0) to 49,896 ha (RCP4.5).

The conversion of unmanaged land (Appendix A.4) follows a similar trajectory across scenarios. Total unmanaged land declines sharply from 939,600 ha in 2020 to between 650,000 and 700,000 ha by 2025. This reduced level remains relatively stable through to 2100, ending between 649,296 ha and 668,979 ha, depending on the scenario.

7. Discussion

This study develops a coupled land-use change-ecohydrological model to assess climate and socioeconomic impacts on agricultural production and water use in multi-seasonal arid and semi-arid agricultural systems. The approach integrates the SWAT + ecohydrological model, which generates spatially distributed potential crop yields (serving as a natural capital layer), with CRAFTY, an ABM simulating land-use change and management decisions. Within the ABM, agricultural agents, representing cropping patterns and management practices, compete based on natural and socioeconomic capitals and agent characteristics. The ecohydrological model was calibrated and its performance evaluated against observed annual yield and irrigation data under full irrigation conditions, demonstrating acceptable agreement given data limitations; while deficit irrigation scenarios were subsequently developed through sensitivity analysis to identify realistic water-saving strategies with limited yield reduction. We conduct a climate change scenario analysis, which projected potential yield increases under scenarios with elevated atmospheric CO_2 levels for wheat, main vegetables, sugarcane, fodder crops, while declines were observed for maize, rice, and other vegetables, suggesting that any declines due to increasing temperatures are counteracted by CO_2 fertilisation effects for some crops but not for others. We also show that irrigation water use reduced at the highest rate for scenarios with the highest CO_2 levels, demonstrating the impact of elevated CO_2 on water use. Finally, we establish the benefit of the coupled model by running the model using potential crop yields under different climate scenarios, static socioeconomic capitals and demand, and business-as-usual agent properties. This demonstrates that even in light of the static socioeconomic capitals and demand, the coupled model results in some adaptation in response to dynamic potential yields.

7.1. Climate change impact on crop yields

Our results indicate that C3 crops, such as wheat, and fodder crops experience increased yields under elevated CO_2 concentrations. This finding aligns with previous studies (Ahmed et al., 2019; Ainsworth and Long, 2021; Elsadek et al., 2024; Rezaei et al., 2023), which consistently report enhanced productivity in C3 crops due to increased

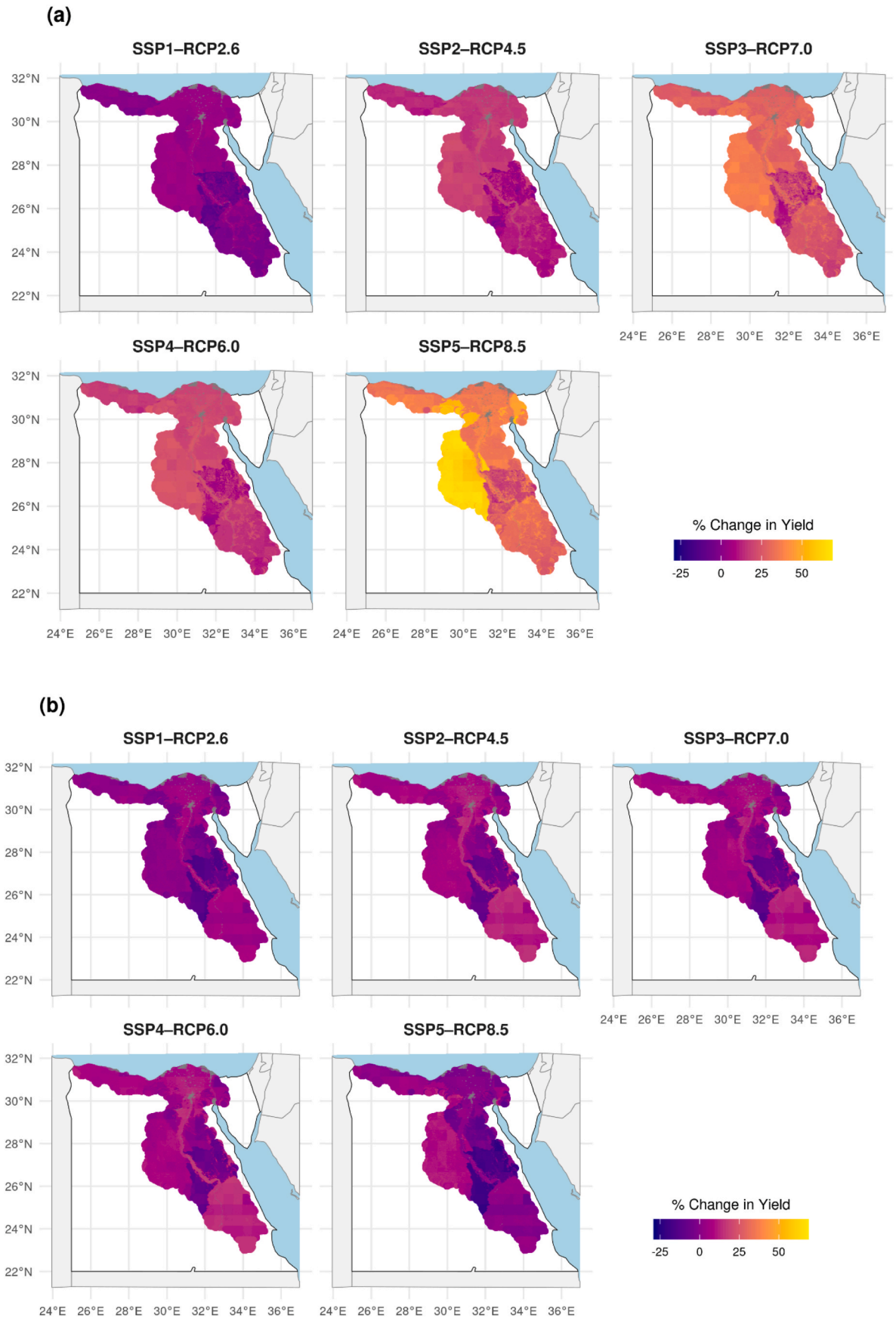

Fig. 7. Spatial change in crop yield under different climate scenarios: Percentage change in yield for (a) wheat and (b) maize between 2020 and 2099. Five-year average yields are used to smooth interannual variability (2020–2024 and 2095–2099).

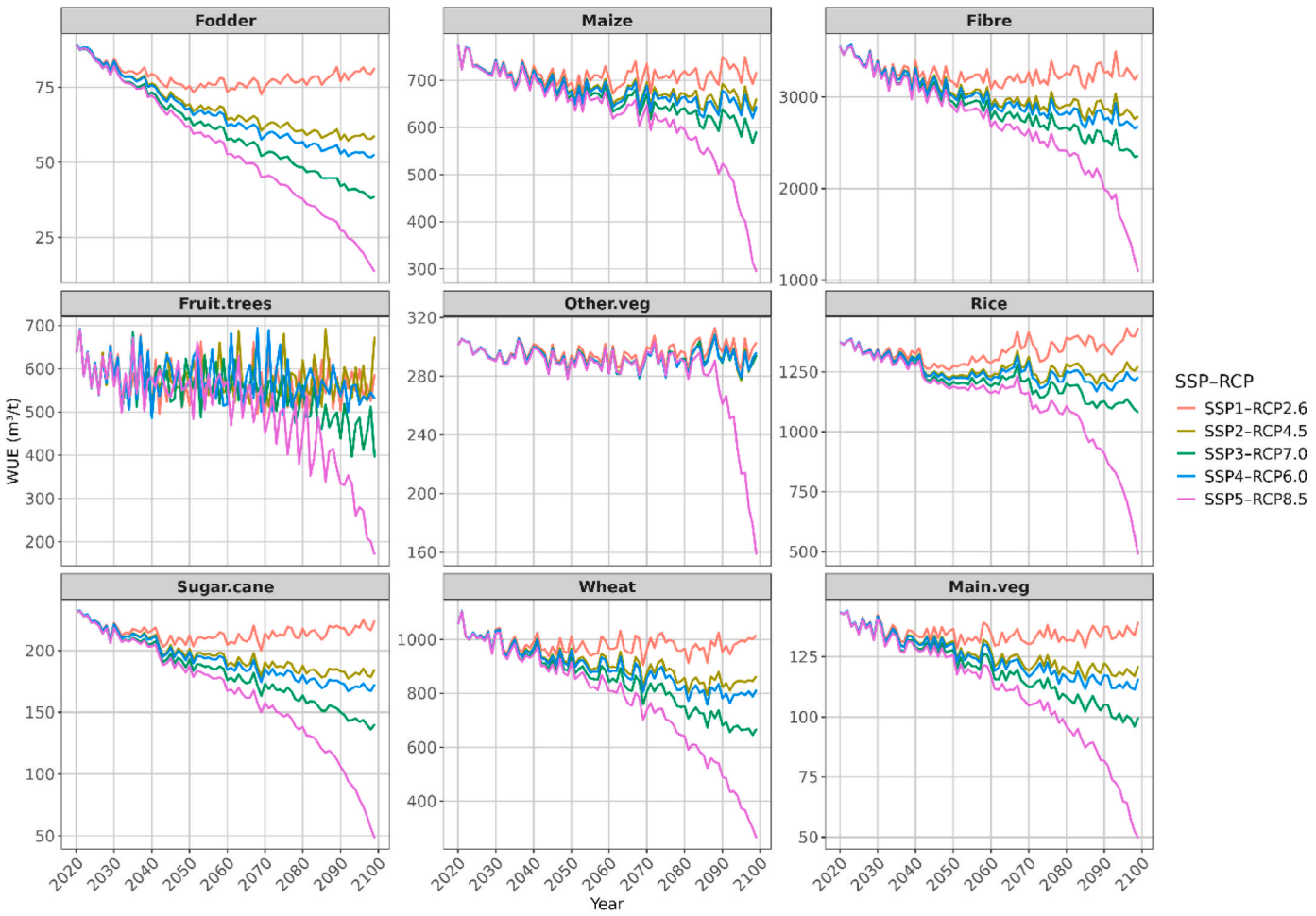

Fig. 8. Trajectories of water use efficiency (WUE) under future climate scenarios: Projected WUE for major crops from 2020 to 2099.

photosynthetic efficiency under elevated CO_2. In contrast, C4 crops, such as maize, show no benefit of elevated CO_2 concentrations, except under drought-stressed conditions (Rezaei et al., 2023). This is consistent with our results, where maize yields increase modestly across most climate scenarios, with slight reductions occurring under scenarios with the highest atmospheric CO_2 concentrations. Since we model potential yields under non-water-stressed conditions, the reduction observed for maize further supports expectations based on physiological crop responses.

A study of the Mediterranean region using the Lund-Potsdam-Jena managed Land (LPJmL) ecohydrological and agro-ecosystem model found yield increases for multiple crops under global warming scenarios ranging from 2 °C to 5 °C (Fader et al., 2016). For sugarcane, yields increased by 30 % and 120 % when comparing 2000–2009 to 2080–2090 under 2 °C and 5 °C scenarios, respectively, using dynamic CO_2 concentrations. Notably, under elevated CO_2, all crops experienced some level of yield gain across all scenarios. In contrast, under constant CO_2 levels, most crops showed yield reductions, typically within 20 %, although some crops, including sugarcane, maintained their yield increases. Broadly, our findings align with these results. However, while Fader et al. (2016) report continuous increases in rice yield across all scenarios, our results show an initial increase followed by a decline, especially under high-emissions scenarios. This discrepancy may stem from differences in climate and CO_2 input data; their scenarios reach a maximum of 720 ppm CO_2 under 5 °C warming, whereas our RCP8.5 scenario reaches 1135 ppm by 2100.

Previous studies assessing climate change impacts on Egyptian agriculture report mixed findings (Elsadek et al., 2024; Gamal et al., 2021; Kheir et al., 2019; Moghazy and Kaluarachchi, 2021; S. M. Mostafa et al., 2021). For instance, Moghazy and Kaluarachchi (2021) used linear regression with climate projections to estimate yield impacts in the Siwa region (Western Desert), projecting reductions of 10.4–27.4 % by 2100 under RCP8.5. However, their model did not include elevated CO_2 effects. In contrast, Elsadek et al. (2024), applying the AquaCrop-GIS model for rice in the Nile Delta, found yield gains under both RCP4.5 and RCP8.5 with elevated CO_2. Their projections show rice yields increasing from 14.5 % in the 2030s to 16.9 % in the 2090s under RCP4.5, while RCP8.5 shows a peak gain of 16.9 % in the 2050s followed by a smaller increase of 1.6 % by the 2090s. Our model also shows an initial yield increase for rice under RCP4.5, peaking around 2070, followed by a decline, resulting in a net gain of just 1.8 % between 2020 and 2099. Moreover, under RCP8.5, rice yields decline by 5.1 % over the modelling period. These differences may reflect the broader geographic scope of our model, which includes southern Egypt, where higher warming is expected. In these areas, the positive effects of CO_2 fertilisation may be outweighed by heat stress more than in the cooler Delta region.

Our results show increases in wheat yield under all scenarios, with the largest gain (36 %) under RCP8.5. Kheir et al. (2019) investigated the effects of sea-level rise, increased temperature, and elevated CO_2 on two wheat cultivars in a Kafr-El-Sheikh, a Nile Delta governorate, using two DSSAT wheat models. Their results showed that a 4 °C temperature increase could reduce yields by up to 18 %, while elevated CO_2 concentrations (400–700 ppm) increased yields by 5–25 %. Although our model does not simulate these specific cultivars and assumes ideal growing conditions with combined climate effects, the general trends

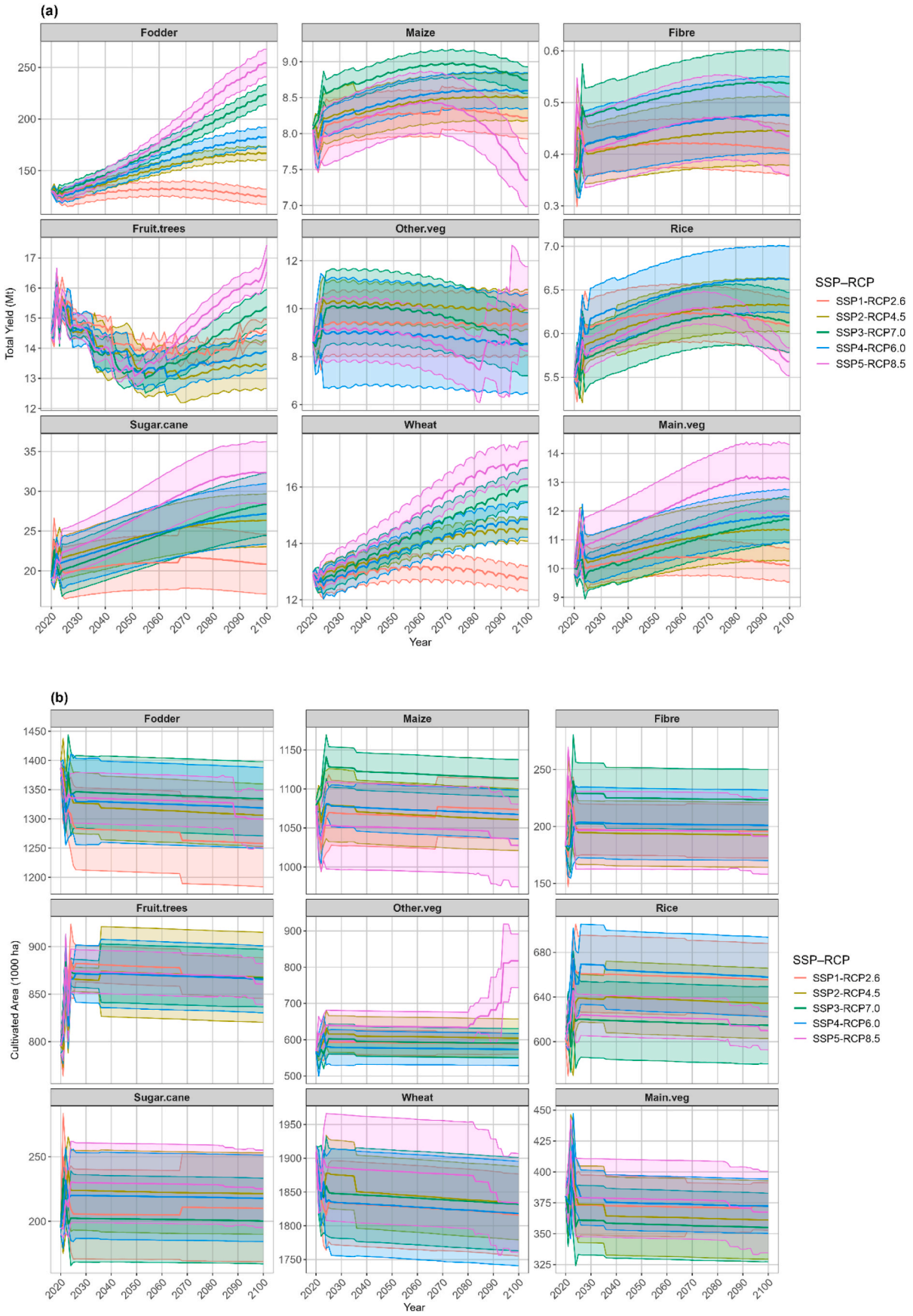

Fig. 9. Projected crop production and cultivated area under future scenarios: (a) Total crop production and (b) total cultivated area for key crops across all scenarios. Solid lines represent the median across 10 initial land use map runs, while shaded ribbons indicate the inter-run standard deviation.

are consistent, demonstrating that elevated CO_2 can offset some of the negative impacts of warming on wheat yield.

Overall, these studies highlight the complex and uncertain nature of climate change impacts on crop yields. Rising temperatures are generally expected to reduce yields, while elevated CO_2 concentrations may offset some of these losses, particularly for C3 crops. Our findings are broadly consistent with this pattern, though rice shows some divergence, likely due to differences in climate sensitivity and spatial variation across Egypt. However, the magnitude of the CO_2 fertilisation effect remains uncertain and may lead to an overestimation of future yield potential, particularly in the absence of nutrient or management constraints (Ainsworth et al., 2025; Q. Cao et al., 2022). Moreover, these positive effects could be offset by interacting stressors such as increasing temperature extremes, drought frequency, and soil degradation, which are not explicitly represented in the current coupled model (Ainsworth et al., 2025).

7.2. Water use under future climate scenarios

Our modelling results show reductions in water use across all scenarios and crops. This trend is generally consistent with other studies that account for both increased temperatures and elevated CO_2 concentrations (Tian et al., 2023; Toreti et al., 2020), where reductions in crop transpiration are primarily attributed to decreased stomatal conductance under elevated CO_2. For example, Fader et al. (2016) analysed irrigation water use for multiple crops across the Mediterranean region and found a net reduction in irrigation demand for most crops included in our simulations, such as temperate cereals (e.g. wheat), potatoes (included under other vegetables), and pulses (included under legumes). In contrast to our results, however, their results showed increased irrigation for sugarcane, citrus, and rice. These differences may reflect the relatively higher dependence on irrigation in our study area compared to the broader Mediterranean average.

Mokhtar et al. (2025) conducted a meta-analysis of WUE responses to elevated CO_2 across various crops and field experiments. They found that C3 crops such as wheat and tomatoes (main vegetables) exhibited consistent improvements in WUE, with increases of up to 40–50 % in some cases. C4 crops, including maize and sugarcane, also showed improvements, albeit to a lesser extent. Similar patterns are observed in Q. Cao et al. (2022), who reported WUE increases of 27.8 % for wheat and 49.7 % for maize under 800 ppm CO_2 in non-drought conditions.

Several studies have explored the impacts of climate change on water use in Egypt, though most focus solely on temperature effects (Gabr, 2023; S. Mostafa et al., 2021). These studies consistently project increases in irrigation demand, such as S. Mostafa et al. (2021), who estimate increases ranging from 6.1 % to 7.3 % for winter crops and 11.7 %–13.2 % for summer crops due to higher evapotranspiration under warming scenarios.

The reductions in irrigation water use observed in our results should be interpreted in the context of how evapotranspiration (ET) is represented within SWAT+. Potential ET generally increases under warmer conditions, while elevated CO_2 reduces stomatal conductance and can lower actual ET. Both processes are simulated internally within the SWAT + crop–water balance and therefore influence crop water demand in the model. As a result, water demand does not rise in direct proportion to temperature increases and may decline for some crops. This behaviour is consistent with the reductions in irrigation requirements that we observe across the climate scenarios.

Overall, our results are in agreement with studies that incorporate both temperture rise and CO_2 fertilisation effects, showing net improvements in water use efficiency under future climate scenarios. However, such integrated modelling studies remain limited for Egypt, highlighting a gap in the regional literature.

7.3. Model evaluation

We use our coupled model implementation to demonstrate the value of coupling a biophysical model with an agent-based land-use change model, under a simplified scenario framework. This example assumes dynamic potential yields driven by climate change, but holds socio-economic capitals, demand, and AFT parameters constant and uniform across scenarios. Despite these simplified assumptions, the model produces notable land-use dynamics, including land abandonment, reclamation, and shifts in crop areas in response to changing yield potentials. For instance, the greatest decline in potential yield is observed for other vegetables under RCP8.5. This yield reduction leads to an expansion in cultivated area for that crop after 2080, accompanied by the re-cultivation of previously abandoned land.

Previous models that couple biophysical and agent-based components (e.g. Du et al., 2020; Harms et al., 2023; O'Keeffe et al., 2018) have primarily focused on irrigation decision-making while limiting endogenous land-use change, despite its central role in adaptation to climate change (e.g. Adly et al., 2018; Boazar et al., 2020; Chouchane et al., 2020). Unlike optimisation-based approaches (e.g. Fikry et al., 2021; Sardo et al., 2024), the coupled LUC-EH model enables land-use change to emerge endogenously by defining initial conditions and allowing land allocation to evolve without imposing prescriptive decision rules.

8. Limitations

Although the model presents some key developments, limited access to high-resolution gauging data and evapotranspiration (ET) measurements constrained the accuracy of model calibration. Such limitations are common in data-scarce regions, where ecohydrological models must often rely on sparse and fragmented monitoring networks (Chawanda et al., 2024). While SWAT + benefits from open-source datasets, global satellite products, and climate model integrations, making it suitable for applications in data-poor regions, the absence of detailed records on irrigation return flows and groundwater abstraction complicates the calibration of key hydrological parameters (Akoko et al., 2021). Although a formal Monte Carlo uncertainty analysis was not performed, uncertainty was addressed through sensitivity analysis and the inclusion of multiple climate scenarios, which capture a broad range of plausible outcomes for crop yield and water use.

The moderate calibration performance for some crops reflects the limited availability and quality of long-term yield and irrigation data in Egypt. Governorate-level statistics provide only coarse spatial and temporal detail, and inconsistencies between years reduce their usefulness for model tuning. As a result, the calibrated parameters are best viewed as capturing general patterns rather than precise field-level responses. This affects the interpretation of scenario results, which should be understood as indicative of broad trends and relative differences between scenarios rather than exact projections of yield or water use.

Urban growth and competition with agricultural land are not explicitly simulated in this version of the model, although CRAFTY has the capacity to represent such processes. These were intentionally excluded to isolate the effects of climate change on agricultural land use. In the context of Egypt, this omission is expected to have limited national-scale implications due to the availability of desert margins suitable for managed agricultural expansion, although localised interactions between urban and agricultural land in the Nile Delta warrant inclusion in future model development.

Egypt's hydrological system is highly complex, involving interactions between surface irrigation infrastructure, subsurface tile drainage, and the widespread reuse of agricultural drainage water (Barnes, 2014). Although SWAT + supports the conceptual separation of surface and groundwater irrigation sources, the current implementation does not explicitly assign or quantify these sources. Furthermore, groundwater withdrawals are not directly modelled, which limits the ability to assess their contribution to aquifer depletion or the risk of

saltwater intrusion in coastal regions and may lead to an underestimation of water scarcity or overestimation of adaptive capacity in groundwater-dependent areas. This is largely due to the absence of openly accessible, regularly updated spatial and temporal datasets describing the structure, operation, and management of irrigation infrastructure, including pumping stations, return flows, and conveyance systems. Incorporating these processes into future model development would substantially improve assessments of groundwater sustainability and irrigation system resilience. In addition, the omission of institutional and governance factors such as water allocation rules, collective management arrangements, and agricultural subsidies constrains the realism of water accounting and limits the direct translation of the results into policy. Incorporating these aspects, alongside improved infrastructure data, would substantially strengthen future assessments of groundwater sustainability and irrigation system resilience.

9. Conclusion

This study demonstrates the value of coupling behavioural and biophysical models to simulate agricultural responses to climate change in arid, multi-seasonal agricultural systems. By linking CRAFTY and SWAT+, we move beyond static impact modelling to explore how cropping patterns and irrigation decisions might shift in response to changing environmental conditions. While this application uses a stylised version of the model with static socioeconomic conditions and demand, it shows that even under stagnant assumptions, agricultural land-use change processes can enhance the interpretation of biophysical responses. These dynamic shifts redistribute cropping patterns in ways that partially offset or amplify climate-driven yield changes. However, the current version does not represent non-agricultural transitions such as urban expansion, which may further influence land availability in future applications.

The results also underscore the potential significance of rising atmospheric CO_2 concentrations, which improve water use efficiency and may benefit the yields of some crops, particularly C3 species such as wheat and fodder crops. However, these gains are not uniform and may be offset by increased heat stress, pointing to the need for cautious interpretation. More broadly, the coupled model offers a transferable and open-access tool for scenario analysis in regions facing similar constraints. Applying the model to fully developed climate–socioeconomic scenarios would allow for more robust exploration of adaptation pathways and the complex interplay between natural and human systems.

CRediT authorship contribution statement

Aimen Sattar: Writing – review & editing, Writing – original draft, Visualization, Software, Methodology, Formal analysis, Data curation, Conceptualization. **Simon Moulds:** Writing – review & editing, Supervision, Methodology, Conceptualization. **Calum Brown:** Writing – review & editing, Supervision, Methodology, Conceptualization. **Mark Rounsevell:** Writing – review & editing, Supervision, Methodology, Conceptualization. **Peter Alexander:** Writing – review & editing, Supervision, Methodology, Conceptualization.

Declaration of generative AI and AI-assisted technologies in the writing process

During the preparation of this work, the authors used ChatGPT by OpenAI to improve readability and language. After using this tool/service, the authors reviewed and edited the content as needed and take full responsibility for the content of the publication.

Funding

This research did not receive any specific grant from funding agencies in the public, commercial, or not-for-profit sectors.

Declaration of competing interest

The authors declare that they have no known competing financial interests or personal relationships that could have appeared to influence the work reported in this paper.

Acknowledgments

This work has made use of the resources provided by the Edinburgh Compute and Data Facility (ECDF) (http://www.ecdf.ed.ac.uk/).

We thank the SWAT + development team, especially Nancy B. Sammons and Chris George, for their technical support and guidance in implementing and troubleshooting the SWAT + model for this application. We also acknowledge Dr. Mohamed Byari for his assistance in applying the CRAFTY model, particularly in resolving issues related to model setup.

Appendix A. Supplementary data

Supplementary data to this article can be found online at https://doi.org/10.1016/j.envsoft.2025.106845.

Data availability

The SWAT + ecohydrological model (version 61.0.2.10) used in this study is open source and can be obtained from its official repository on GitHub (https://github.com/swat-model/swatplus/releases). The CRAFTY land-use modelling framework is also open source and available via its GitHub repository (https://github.com/CRAFTY-ABM/CRAFTY_User_Interface/tree/master/CraftyProject). All datasets used in this study are publicly available, and their sources are cited within the manuscript or included in the Appendices. The custom code developed for data processing, model input preparation, and coupling of SWAT+ and CRAFTY is available from the corresponding author upon reasonable request.

References

Abdelhafez, A.A., Metwalley, S.M., Abbas, H.H., 2020. Irrigation: water resources, types and common problems in Egypt. In: Omran, E.-S.E., Negm, A.M. (Eds.), Technological and Modern Irrigation Environment in Egypt: Best Management Practices & Evaluation. Springer International Publishing, pp. 15–34. https://doi.org/10.1007/978-3-030-30375-4_2.

Adly, N., Noiser, S., Kassem, N., Mahrous, M., Salah, R., 2018. Modelling the optimal cropping pattern to 2030 under different climate change scenarios: a study on Egypt. African J. Agric. Res. Econ. 13 (3), 224–239. Retrieved 2018-09, from. https://ageconsearch.umn.edu/record/284987/files/3.-Adly-et-al.pdf.

Adriansen, H.K., 2009. Land reclamation in Egypt: a study of life in the new lands. Geoforum 40 (4), 664–674. https://doi.org/10.1016/j.geoforum.2009.05.006.

Ahmed, M., Stöckle, C.O., Nelson, R., Higgins, S., Ahmad, S., Raza, M.A., 2019. Novel multimodel ensemble approach to evaluate the sole effect of elevated CO2 on winter wheat productivity. Sci. Rep. 9 (1), 7813. https://doi.org/10.1038/s41598-019-44251-x.

Ainsworth, E.A., Long, S.P., 2021. 30 years of free-air carbon dioxide enrichment (FACE): what have we learned about future crop productivity and its potential for adaptation? Glob. Change Biol. 27 (1), 27–49. https://doi.org/10.1111/gcb.15375.

Ainsworth, E.A., Sanz-Saez, A., Leisner, C.P., 2025. Crops and rising atmospheric CO2: friends or foes? Phil. Trans. Biol. Sci. 380, 20240230. https://doi.org/10.1098/rstb.2024.0230, 1927.

Akoko, G., Le, T.H., Gomi, T., Kato, T., 2021. A review of SWAT model application in Africa. Water 13 (9). https://doi.org/10.3390/w13091313.

Alam, M.F., McClain, M., Sikka, A., Pande, S., 2022. Understanding human–water feedbacks of interventions in agricultural systems with agent based models: a review. Environ. Res. Lett. 17 (10). https://doi.org/10.1088/1748-9326/ac91e1.

Arnold, J.G., Bieger, K., White, M.J., Srinivasan, R., Dunbar, J.A., Allen, P.M., 2018. Use of decision tables to simulate management in SWAT+. Water 10 (6). https://doi.org/10.3390/w10060713.

Arnold, J.G., Srinivasan, R., Muttiah, R.S., Williams, J.R., 1998. Large area hydrologic modeling and assessment part I: model development. JAWRA J. Am. Water Res. Associat. 34 (1), 73–89. https://doi.org/10.1111/j.1752-1688.1998.tb05961.x.

Barnes, J., 2014. Mixing waters: the reuse of agricultural drainage water in Egypt. Geoforum 57, 181–191. https://doi.org/10.1016/j.geoforum.2012.11.019.

Berger, T., Birner, R., McCarthy, N., DíAz, J., Wittmer, H., 2007. Capturing the complexity of water uses and water users within a multi-agent framework. Water Resour. Manag. 21 (1), 129–148. https://doi.org/10.1007/s11269-006-9045-z.

Bieger, K., Arnold, J.G., Rathjens, H., White, M.J., Bosch, D.D., Allen, P.M., Volk, M., Srinivasan, R., 2017. Introduction to SWAT+, A completely restructured version of the soil and water assessment tool. JAWRA J. Am. Water Res. Associat. 53 (1), 115–130. https://doi.org/10.1111/1752-1688.12482.

Blanco, V., Holzhauer, S., Brown, C., Lagergren, F., Vulturius, G., Lindeskog, M., Rounsevell, M.D.A., 2017. The effect of forest owner decision-making, climatic change and societal demands on land-use change and ecosystem service provision in Sweden. Ecosyst. Serv. 23, 174–208. https://doi.org/10.1016/j.ecoser.2016.12.003.

Boazar, M., Abdeshahi, A., Yazdanpanah, M., 2020. Changing rice cropping patterns among farmers as a preventive policy to protect water resources. J. Environ. Plann. Manag. 63 (14), 2484–2500. https://doi.org/10.1080/09640568.2020.1729705.

Brown, C., Millington, J., Rounsevell, M., 2023. Assessing the quality of land system models: moving from valibration to evaludation. Socio-Environ. Sys. Modell. 5, 18434. https://doi.org/10.18174/sesmo.18434.

Brown, C., Seo, B., Alexander, P., Burton, V., Chacón-Montalván, E.A., Dunford, R., Merkle, M., Harrison, P.A., Prestele, R., Robinson, E.L., Rounsevell, M., 2022. Agent-based modeling of alternative futures in the British land use system. Earths Future 10 (11). https://doi.org/10.1029/2022ef002905.

Brown, C., Seo, B., Rounsevell, M., 2019. Societal breakdown as an emergent property of large-scale behavioural models of land use change. Earth Syst. Dyn. 10 (4), 809–845. https://doi.org/10.5194/esd-10-809-2019.

Canales, M., Castilla-Rho, J., Rojas, R., Vicuña, S., Ball, J., 2024. Agent-based models of groundwater systems: a review of an emerging approach to simulate the interactions between groundwater and society. Environ. Model. Software 175. https://doi.org/10.1016/j.envsoft.2024.105980.

Cao, Q., Li, G., Liu, F., 2022. Elevated CO(2) enhanced water use efficiency of wheat to progressive drought stress but not on maize. Front. Plant Sci. 13, 953712. https://doi.org/10.3389/fpls.2022.953712.

Cao, Z., Wang, S., Luo, P., Xie, D., Zhu, W., 2022. Watershed ecohydrological processes in a changing environment: opportunities and challenges. Water 14 (9), 1502. https://www.mdpi.com/2073-4441/14/9/1502.

CAPMAS, 2025. Central Agency for Public Mobilization and Statistics: Various Annual Reports. https://www.capmas.gov.eg/HomePage.aspx.

Čerkasova, N., White, M., Arnold, J., Bieger, K., Allen, P., Gao, J., Gambone, M., Meki, M., Kiniry, J., Gassman, P.W., 2023. Field scale SWAT+ modeling of corn and soybean yields for the contiguous United States: national Agroecosystem model development. Agric. Syst. 210. https://doi.org/10.1016/j.agsy.2023.103695.

Chawanda, C.J., Nkwasa, A., Thiery, W., van Griensven, A., 2024. Combined impacts of climate and land-use change on future water resources in Africa. Hydrol. Earth Syst. Sci. 28 (1), 117–138. https://doi.org/10.5194/hess-28-117-2024.

Chouchane, H., Krol, M.S., Hoekstra, A.Y., 2020. Changing global cropping patterns to minimize national blue water scarcity. Hydrol. Earth Syst. Sci. 24 (6), 3015–3031. https://doi.org/10.5194/hess-24-3015-2020.

Copernicus Climate Change Service, 2019. Land cover classification gridded maps from 1992 to present derived from satellite observation. Copernicus Clim. Change Serv. (C3S) Clim. Data Store (CDS). https://doi.org/10.24381/cds.006f2c9a.

Delhey, J., Dragolov, G., Boehnke, K., 2023. Social cohesion in international comparison: a review of key measures and findings. KZfSS Kölner Zeitschrift für Soziologie und Sozialpsychologie 75 (1), 95–120. https://doi.org/10.1007/s11577-023-00891-6.

Dlamini, L., Crespo, O., van Dam, J., Kooistra, L., 2023. A global systematic review of improving crop model estimations by assimilating remote sensing data: implications for small-scale agricultural systems. Remote Sens. 15 (16). https://doi.org/10.3390/rs15164066.

Du, E., Tian, Y., Cai, X., Zheng, Y., Li, X., Zheng, C., 2020. Exploring spatial heterogeneity and temporal dynamics of human-hydrological interactions in large river basins with intensive agriculture: a tightly coupled, fully integrated modeling approach. J. Hydrol. 591. https://doi.org/10.1016/j.jhydrol.2020.125313.

El-Beltagy, A., Madkour, M., 2012. Impact of climate change on arid lands agriculture. Agric. Food Secur. 1 (1), 3. https://doi.org/10.1186/2048-7010-1-3.

El Fartassi, I., Milne, A.E., Metcalfe, H., El Alami, R., Diarra, A., Alonso-Chavez, V., Zawadzka, J., Waine, T.W., Corstanje, R., 2025. An agent-based model of farmer decision making: application to shared water resources in Arid and semi-arid regions. Agric. Water Manag. 310, 109357. https://doi.org/10.1016/j.agwat.2025.109357.

Elsadek, E.A., Zhang, K., Hamoud, Y.A., Mousa, A., Awad, A., Abdallah, M., Shaghaleh, H., Hamad, A.A.A., Jamil, M.T., Elbeltagi, A., 2024. Impacts of climate change on rice yields in the Nile River Delta of Egypt: a large-scale projection analysis based on CMIP6. Agric. Water Manag. 292, 108673. https://doi.org/10.1016/j.agwat.2024.108673.

Elsayed, M.L., Elkot, A.F., Noreldin, T., Richard, B., Qi, A., Shabana, Y.M., Saleh, S.M., Fitt, B.D.L., Kheir, A.M.S., 2025. Optimizing wheat yield and water productivity under water scarcity: a modeling approach for irrigation and cultivar selection across different agro-climatic zones of Egypt. Agric. Water Manag. 317, 109668. https://doi.org/10.1016/j.agwat.2025.109668.

Fader, M., Shi, S., von Bloh, W., Bondeau, A., Cramer, W., 2016. Mediterranean irrigation under climate change: more efficient irrigation needed to compensate for increases in irrigation water requirements. Hydrol. Earth Syst. Sci. 20 (2), 953–973. https://doi.org/10.5194/hess-20-953-2016.

FAO, 2014. Egyptian Clover (Trifolium alexandrinum). Food Agric. Organiz. United Nations. https://openknowledge.fao.org/server/api/core/bitstreams/947fa627-c9f2-4f67-b725-e0ef30d220c7/content.

Feng, X., Tian, H., Cong, J., Zhao, C., 2023. A method review of the climate change impact on crop yield. Front. For. Glob. Change 6. https://doi.org/10.3389/ffgc.2023.1198186.

Fikry, I., Eltawil, A., Gheith, M., 2021. A Robust crop rotation optimization model with water scarcity and net return uncertainty considerations. IEEE Access 9, 128938–128950. https://doi.org/10.1109/access.2021.3113125.

Food and Agriculture Organization of the United Nations, 2005. Fertilizer Use by Crop in Egypt. FAO. https://openknowledge.fao.org/server/api/core/bitstreams/b3d837e2-48c9-4adc-aa36-797bf45e5f68/content.

Gabr, M.E., 2023. Impact of climatic changes on future irrigation water requirement in the Middle East and North Africa's region: a case study of upper Egypt. Appl. Water Sci. 13 (7), 158. https://doi.org/10.1007/s13201-023-01961-y.

Gado, T.A., El-Agha, D.E., 2021. Climate change impacts on water balance in Egypt and opportunities for adaptations. In: Agro-Environmental Sustainability in MENA Regions, pp. 13–47. https://doi.org/10.1007/978-3-030-78574-1_2.

Gamal, G., Samak, M., Shahba, M., 2021. The possible impacts of different global warming levels on major crops in Egypt. Atmosphere 12 (12), 1589. https://www.mdpi.com/2073-4433/12/12/1589.

Gleeson, T., 2018. *GLobal HYdrogeology MaPS (GLHYMPS) of permeability and porosity* Version V1) [GLobal HYdrogeology MaPS (GLHYMPS) of permeability and porosity are based on a high-resolution global lithology map that differentiates fine and coarse-grained sediments and sedimentary rocks. The average polygon size is ~100 km2. The maps are distributed as a geodatabase folder (GDB) and can be viewed using ArcGIS or similar software. Borealis. https://doi.org/10.5683/SP2/DLGXYO.

Grigorieva, E., Livenets, A., Stelmakh, E., 2023. Adaptation of agriculture to climate change: a scoping review. Climate 11 (10). https://doi.org/10.3390/cli11100202.

Harms, J.Z., Malard-Adam, J.J., Adamowski, J.F., Sharma, A., Nkwasa, A., 2023. Dynamically coupling system dynamics and SWAT+ models using Tinamït: application of modular tools for coupled human–water system models. Hydrol. Earth Syst. Sci. 27 (8), 1683–1693. https://doi.org/10.5194/hess-27-1683-2023.

Hengl, T., Mendes de Jesus, J., Heuvelink, G.B., Ruiperez Gonzalez, M., Kilibarda, M., Blagotic, A., Shangguan, W., Wright, M.N., Geng, X., Bauer-Marschallinger, B., Guevara, M.A., Vargas, R., MacMillan, R.A., Batjes, N.H., Leenaars, J.G., Ribeiro, E., Wheeler, I., Mantel, S., Kempen, B., 2017. SoilGrids250m: global gridded soil information based on machine learning. PLoS One 12 (2), e0169748. https://doi.org/10.1371/journal.pone.0169748.

Holzworth, D.P., Huth, N.I., deVoil, P.G., Zurcher, E.J., Herrmann, N.I., McLean, G., Chenu, K., van Oosterom, E.J., Snow, V., Murphy, C., Moore, A.D., Brown, H., Whish, J.P.M., Verrall, S., Fainges, J., Bell, L.W., Peake, A.S., Poulton, P.L., Hochman, Z., Keating, B.A., 2014. APSIM – evolution towards a new generation of agricultural systems simulation. Environ. Model. Software 62, 327–350. https://doi.org/10.1016/j.envsoft.2014.07.009.

Hou, J., Van Dijk, A.I.J.M., Renzullo, L.J., Larraondo, P.R., 2024. GloLakes: water storage dynamics for 27 000 lakes globally from 1984 to present derived from satellite altimetry and optical imaging. Earth Syst. Sci. Data 16 (1), 201–218. https://doi.org/10.5194/essd-16-201-2024.

Huber, R., Bakker, M., Balmann, A., Berger, T., Bithell, M., Brown, C., Grêt-Regamey, A., Xiong, H., Le, Q.B., Mack, G., Meyfroidt, P., Millington, J., Müller, B., Polhill, J.G., Sun, Z., Seidl, R., Troost, C., Finger, R., 2018. Representation of decision-making in European agricultural agent-based models. Agric. Syst. 167, 143–160. https://doi.org/10.1016/j.agsy.2018.09.007.

Humanitarian OpenStreetMap Team (HOT), 2024. Egypt waterways (OpenStreetMap export). https://data.humdata.org/dataset/hotosm_egy_waterways.

Huscroft, J., Gleeson, T., Hartmann, J., Börker, J., 2018. *Compiling and Mapping Global Permeability of the Unconsolidated and Consolidated Earth: Global Hydrogeology Maps 2.0 (GLHYMPS 2.0). [Supporting Data]* Version V1) [Global Hydrogeology Maps (GLHYMPS) of Permeability and Porosity are Based on a high-resolution Global Lithology Map that Differentiates Fine and coarse-grained Sediments and Sedimentary Rocks. the Average Polygon Size is ~100 km2. the Maps are Distributed as an ESRI Shapefile and can be Viewed Using Arcgis, QGIS (Free), or Similar Software. Borealis. https://doi.org/10.5683/SP2/TTJNIU.

Jägermeyr, J., Müller, C., Ruane, A.C., Elliott, J., Balkovic, J., Castillo, O., Faye, B., Foster, I., Folberth, C., Franke, J.A., Fuchs, K., Guarin, J.R., Heinke, J., Hoogenboom, G., Iizumi, T., Jain, A.K., Kelly, D., Khabarov, N., Lange, S., Rosenzweig, C., 2021. Climate impacts on global agriculture emerge earlier in new generation of climate and crop models. Nat. Food 2 (11), 873–885. https://doi.org/10.1038/s43016-021-00400-y.

Kheir, A.M.S., El Baroudy, A., Aiad, M.A., Zoghdan, M.G., Abd El-Aziz, M.A., Ali, M.G.M., Fullen, M.A., 2019. Impacts of rising temperature, carbon dioxide concentration and sea level on wheat production in North Nile delta. Sci. Total Environ. 651, 3161–3173. https://doi.org/10.1016/j.scitotenv.2018.10.209.

Kimpton, L., Challenor, P., Salter, J., 2024. Uncertainty quantification for agent based models: a tutorial. arXiv preprint arXiv:2409.16776.

Koch, J., Leimbach, M., 2023. SSP economic growth projections: major changes of key drivers in integrated assessment modelling. Ecol. Econ. 206. https://doi.org/10.1016/j.ecolecon.2023.107751.

Lange, S., Büchner, M., 2021. *ISIMIP3b bias-adjusted atmospheric climate input data* Version 1.1) ISIMIP Repository. https://doi.org/10.48364/ISIMIP.842396.1.

López-Ballesteros, A., Nielsen, A., Castellanos-Osorio, G., Trolle, D., Senent-Aparicio, J., 2023. DSOLMap, a novel high-resolution global digital soil property map for the SWAT + model: development and hydrological evaluation. Catena 231. https://doi.org/10.1016/j.catena.2023.107339.

Malhi, G.S., Kaur, M., Kaushik, P., 2021. Impact of climate change on agriculture and its mitigation strategies: a review. Sustainability 13 (3), 1318. https://www.mdpi.com/2071-1050/13/3/1318.

McDermid, S., Nocco, M., Lawston-Parker, P., Keune, J., Pokhrel, Y., Jain, M., Jägermeyr, J., Brocca, L., Massari, C., Jones, A.D., Vahmani, P., Thiery, W., Yao, Y., Bell, A., Chen, L., Dorigo, W., Hanasaki, N., Jasechko, S., Lo, M.-H., Yokohata, T., 2023. Irrigation in the Earth system. Nat. Rev. Earth Environ. 4 (7), 435–453. https://doi.org/10.1038/s43017-023-00438-5.

Mehareb, E.M., El-Shafai, A.M.A., Fouz, F.M.A., 2021. History and current status of sugarcane breeding in Egypt. Sugar Tech 24 (1), 267–271. https://doi.org/10.1007/s12355-021-01010-5.

Meijer, J.R., Huijbregts, M.A.J., Schotten, K.C.G.J., Schipper, A.M., 2018. Global patterns of current and future road infrastructure. Environ. Res. Lett. 13 (6). https://doi.org/10.1088/1748-9326/aabd42.

Meinshausen, M., Nicholls, Z.R.J., Lewis, J., Gidden, M.J., Vogel, E., Freund, M., Beyerle, U., Gessner, C., Nauels, A., Bauer, N., Canadell, J.G., Daniel, J.S., John, A., Krummel, P.B., Luderer, G., Meinshausen, N., Montzka, S.A., Rayner, P.J., Reimann, S., Wang, R.H.J., 2020. The shared socio-economic pathway (SSP) greenhouse gas concentrations and their extensions to 2500. Geosci. Model Dev. (GMD) 13 (8), 3571–3605. https://doi.org/10.5194/gmd-13-3571-2020.

Messager, M.L., Lehner, B., Grill, G., Nedeva, I., Schmitt, O., 2016. Estimating the volume and age of water stored in global lakes using a geo-statistical approach. Nat. Commun. 7 (1), 13603. https://doi.org/10.1038/ncomms13603.

Mijic, A., Liu, L., O'Keeffe, J., Dobson, B., Chun, K.P., 2023. A meta-model of socio-hydrological phenomena for sustainable water management. Nat. Sustain. 7 (1), 7–14. https://doi.org/10.1038/s41893-023-01240-3.

Millington, J.D.A., Katerinchuk, V., Silva, R.F. B.d., Victoria, D.d.C., Batistella, M., 2021. Modelling drivers of Brazilian agricultural change in a telecoupled world. Environ. Model. Software 139. https://doi.org/10.1016/j.envsoft.2021.105024.

Moghazy, N.H., Kaluarachchi, J.J., 2021. Impact of climate change on agricultural development in a closed groundwater-driven Basin: a case Study of the Siwa Region, Western desert of Egypt. Sustainability 13 (3).

Mokhtar, A., He, H., Attaher, S., Salem, A., Alam, M., 2025. Optimizing water-use efficiency under elevated CO_2: a meta-analysis of crop type, soil modulation, and enrichment methods. Agric. Water Manag. 309, 109312. https://doi.org/10.1016/j.agwat.2025.109312.

Mostafa, S., Wahed, O., El-Nashar, W., El-Marsafawy, S., Zeleňáková, M., Abd-Elhamid, H., 2021. Potential climate change impacts on water resources in Egypt. Water 13 (12). https://doi.org/10.3390/w13121715.

Mostafa, S.M., Wahed, O., El-Nashar, W.Y., El-Marsafawy, S.M., Abd-Elhamid, H.F., 2021. Impact of climate change on water resources and crop yield in the Middle Egypt region. AQUA - Water Infrastruct. Ecosys. Soc. 70 (7), 1066–1084. https://doi.org/10.2166/aqua.2021.019.

Murray-Rust, D., Brown, C., van Vliet, J., Alam, S.J., Robinson, D.T., Verburg, P.H., Rounsevell, M., 2014. Combining agent functional types, capitals and services to model land use dynamics. Environ. Model. Software 59, 187–201. https://doi.org/10.1016/j.envsoft.2014.05.019.

Nguyen, T.V., Dietrich, J., Dang, T.D., Tran, D.A., Van Doan, B., Sarrazin, F.J., Abbaspour, K., Srinivasan, R., 2022. An interactive graphical interface tool for parameter calibration, sensitivity analysis, uncertainty analysis, and visualization for the Soil and Water assessment tool. Environ. Model. Software 156. https://doi.org/10.1016/j.envsoft.2022.105497.

Nour, S.E., 2020. Grabbing from below: a study of land reclamation in Egypt. Rev. Afr. Polit. Econ. 46 (162), 549–566. https://doi.org/10.1080/03056244.2019.1755190.

O'Keeffe, J., Moulds, S., Bergin, E., Brozović, N., Mijic, A., Buytaert, W., 2018. Including farmer irrigation behavior in a sociohydrological modeling framework with application in North India. Water Resour. Res. 54 (7), 4849–4866. https://doi.org/10.1029/2018wr023038.

OAMDI, 2023. Harmonized Household Income and Expenditure Surveys (HHIES). HIECS 2019/2020 Econ. Res. Forum (ERF), Version 3.0. http://www.erfdataportal.com/index.php/catalog.

Ortiz-Bobea, A., Ault, T.R., Carrillo, C.M., Chambers, R.G., Lobell, D.B., 2021. Anthropogenic climate change has slowed global agricultural productivity growth. Nat. Clim. Change 11 (4), 306–312. https://doi.org/10.1038/s41558-021-01000-1.

Pianosi, F., Beven, K., Freer, J., Hall, J.W., Rougier, J., Stephenson, D.B., Wagener, T., 2016. Sensitivity analysis of environmental models: a systematic review with practical workflow. Environ. Model. Software 79, 214–232. https://doi.org/10.1016/j.envsoft.2016.02.008.

Pignotti, G., Rathjens, H., Cibin, R., Chaubey, I., Crawford, M., 2017. Comparative analysis of HRU and grid-based SWAT models. Water 9 (4). https://doi.org/10.3390/w9040272.

Rezaei, E.E., Webber, H., Asseng, S., Boote, K., Durand, J.L., Ewert, F., Martre, P., MacCarthy, D.S., 2023. Climate change impacts on crop yields. Nat. Rev. Earth Environ. 4 (12), 831–846. https://doi.org/10.1038/s43017-023-00491-0.

Sardo, M., Chiarelli, D.D., Ceragioli, F., Rulli, M.C., 2024. Optimized crop distributions in Egypt increase crop productivity and nutritional standards, reducing the irrigation water requirement. Sci. Total Environ. 951, 175202. https://doi.org/10.1016/j.scitotenv.2024.175202.

Sattar, A., Brown, C., Rounsevell, M., Alexander, P., 2024. Typology analysis of Egyptian agricultural households reveals increasing income diversification and abandonment of agricultural activities. Agric. Syst. 218, 104000. https://doi.org/10.1016/j.agsy.2024.104000.

Schrieks, T., Botzen, W.J.W., Wens, M., Haer, T., Aerts, J.C.J.H., 2021. Integrating behavioral theories in agent-based models for agricultural drought risk assessments. Front. Water 3. https://doi.org/10.3389/frwa.2021.686329.

Smits, J., Permanyer, I., 2019. The subnational human development database. Sci. Data 6, 190038. https://doi.org/10.1038/sdata.2019.38.

Steduto, P., Hsiao, T.C., Raes, D., Fereres, E., 2009. AquaCrop—The FAO crop model to simulate yield response to water: I. Concepts and underlying principles. Agron. J. 101 (3), 426–437. https://doi.org/10.2134/agronj2008.0139s.

Streefkerk, I.N., de Bruijn, J., Haer, T., Van Loon, A.F., Quichimbo, E.A., Wens, M., Hassaballah, K., Aerts, J.C.J.H., 2023. A coupled agent-based model to analyse human-drought feedbacks for agropastoralists in dryland regions. Front. Water 4. https://doi.org/10.3389/frwa.2022.1037971.

Su, X., Chen, M., 2022. Econometric approaches that consider farmers' adaptation in estimating the impacts of climate change on agriculture: a review. Sustainability 14 (21). https://doi.org/10.3390/su142113700.

Tian, X., Dong, J., Jin, S., He, H., Yin, H., Chen, X., 2023. Climate change impacts on regional agricultural irrigation water use in semi-arid environments. Agric. Water Manag. 281, 108239. https://doi.org/10.1016/j.agwat.2023.108239.

Toreti, A., Deryng, D., Tubiello, F.N., Müller, C., Kimball, B.A., Moser, G., Boote, K., Asseng, S., Pugh, T.A.M., Vanuytrecht, E., Pleijel, H., Webber, H., Durand, J.-L., Dentener, F., Ceglar, A., Wang, X., Badeck, F., Lecerf, R., Wall, G.W., Rosenzweig, C., 2020. Narrowing uncertainties in the effects of elevated CO2 on crops. Nat. Food 1 (12), 775–782. https://doi.org/10.1038/s43016-020-00195-4.

Tucker, S., Xu, Y., 2023. Fairness, (perception of) inequality, and redistribution preferences. J. Econ. Surv. 37 (5), 1529–1533. https://doi.org/10.1111/joes.12582.

USDA Agricultural Research Service, 2020. *SWAT+ Input/Output Documentation: Version 2.0*. USDA-ARS Grassland. Soil and Water Research Laboratory. https://swat.tamu.edu/media/115579/usda_ars_swatplus_io_doc2020.pdf.

Verkaik, J., Sutanudjaja, E.H., Oude Essink, G.H.P., Lin, H.X., Bierkens, M.F.P., 2024. GLOBGM v1.0: a parallel implementation of a 30 arcsec PCR-GLOBWB-MODFLOW global-scale groundwater model. Geosci. Model Dev. (GMD) 17 (1), 275–300. https://doi.org/10.5194/gmd-17-275-2024.

Wang, R., Bowling, L.C., Cherkauer, K.A., Cibin, R., Her, Y., Chaubey, I., 2017. Biophysical and hydrological effects of future climate change including trends in CO2, in the St. Joseph River watershed, Eastern Corn belt. Agric. Water Manag. 180, 280–296. https://doi.org/10.1016/j.agwat.2016.09.017.

Wang, T., Sun, F., 2022. Global gridded GDP data set consistent with the shared socioeconomic pathways. Sci. Data 9 (1), 221. https://doi.org/10.1038/s41597-022-01300-x.

Wang, X., Meng, X., Long, Y., 2022. Projecting 1 km-grid population distributions from 2020 to 2100 globally under shared socioeconomic pathways. Sci. Data 9 (1), 563. https://doi.org/10.1038/s41597-022-01675-x.

Williams, J.R., Jones, C.A., Dyke, P.T., 1984. A modeling approach to determining the relationship between erosion and soil productivity. Transact. ASAE 27 (1), 129–144.

Yamazaki, D., Ikeshima, D., Tawatari, R., Yamaguchi, T., O'Loughlin, F., Neal, J.C., Sampson, C.C., Kanae, S., Bates, P.D., 2017. A high-accuracy map of global terrain elevations. Geophys. Res. Lett. 44 (11), 5844–5853. https://doi.org/10.1002/2017gl072874.

You, Y., Wang, Y., Fan, X., Dai, Q., Yang, G., Wang, W., Chen, D., Hu, X., 2024. Progress in joint application of crop models and hydrological models. Agric. Water Manag. 295. https://doi.org/10.1016/j.agwat.2024.108746.

Yukimoto, S., Kawai, H., Koshiro, T., Oshima, N., Yoshida, K., Urakawa, S., Tsujino, H., Deushi, M., Tanaka, T., Hosaka, M., Yabu, S., Yoshimura, H., Shindo, E., Mizuta, R., Obata, A., Adachi, Y., Ishii, M., 2019. The meteorological research Institute Earth system model version 2.0, MRI-ESM2.0: Description and basic evaluation of the physical component. J. Meteorol. Soc. Jpn. Ser. II 97 (5), 931–965. https://doi.org/10.2151/jmsj.2019-051.

Zhang, Y., Qi, J., Pan, D., Marek, G.W., Zhang, X., Feng, P., Liu, H., Li, B., Ding, B., Brauer, D.K., Srinivasan, R., Chen, Y., 2022. Development and testing of a dynamic CO2 input method in SWAT for simulating long-term climate change impacts across various climatic locations. J. Hydrol. 614, 128544. https://doi.org/10.1016/j.jhydrol.2022.128544.

Zittis, G., Almazroui, M., Alpert, P., Ciais, P., Cramer, W., Dahdal, Y., Fnais, M., Francis, D., Hadjinicolaou, P., Howari, F., Jrrar, A., Kaskaoutis, D.G., Kulmala, M., Lazoglou, G., Mihalopoulos, N., Lin, X., Rudich, Y., Sciare, J., Stenchikov, G., Lelieveld, J., 2022. Climate change and weather extremes in the Eastern Mediterranean and Middle East. Rev. Geophys. 60 (3). https://doi.org/10.1029/2021rg000762.

Zou, H., Marshall, L., Sharma, A., 2023. Characterizing errors using satellite Metadata for eco-hydrological model calibration. Water Resour. Res. 59 (9). https://doi.org/10.1029/2022WR033978 e2022WR033978.